Enhancement of superconductivity near the ferromagnetic quantum critical point in UCoGe

Master Thesis in Physics
Amsterdam, May 2009
under supervision of Dr. A. de Visser

Erik Slooten

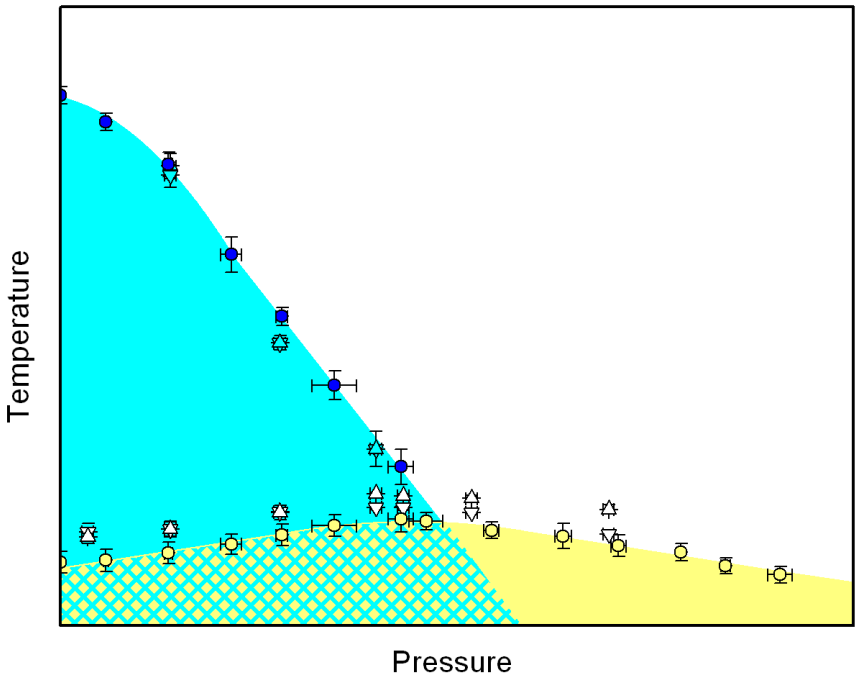

Van der Waals-Zeeman Instituut
Valckenierstraat 65
1018 XE Amsterdam
Faculteit der Natuurwetenschappen, Wiskunde en Informatica

Universiteit van Amsterdam

"Be a man, fix the glitch, just remember life's a bitch"

Motörhead - Life's a Bitch (2004)

Abstract

For a long time it was thought that superconductivity and ferromagnetism exclude each other, since the parallel pairing of spins in ferromagnetic order impedes Cooper pair forming with opposite spins. However recently a family of ferromagnetic superconductors has been discovered, one of them is UCoGe. In these metallic ferromagnets it is expected that spin fluctuations mediate superconductivity by pairing electrons in triplet states. UCoGe enters the ferromagnetic state at $T_C = 3$ K and superconductivity sets in at $T_{sc} = 0.6$ K. At ambient pressure this material is close to a ferromagnetic quantum critical point. In this Master thesis we present the results of our investigation of the pressure temperature phase diagram of UCoGe. Hydrostatic pressure was applied using a clamp-cell technique and the pressure temperature phase diagram was investigated by means of AC-susceptibility and resistivity measurements in the temperature range 0.25-5 K. For $p > 4$ kbar T_C is suppressed at a rate of -0.24 K/kbar and vanishes at a critical pressure $p_c = 14$ kbar. Superconductivity is enhanced near the critical pressure. As a function of pressure T_{sc} increases to a maximum of 0.8 K at 11.6 kbar. This is the pressure at which T_C becomes lower than T_{sc}. Above this pressure T_{sc} decreases steadily. Superconductivity persists throughout the entire pressure range measured (up to 22 kbar). Unlike in other superconducting ferromagnets superconductivity does not vanish together with magnetism. Upper critical field measurements show remarkably large values of $B_{c2}(0)$ (up to three times the ambient pressure value near p_c) on both sides of p_c providing solid evidence for triplet superconductivity throughout the entire pressure range.

Contents

1 Introduction

Since the discovery of superconductivity in 1911 by Kamerlingh Onnes [1] and its successful explanation by Bardeen, Cooper and Schrieffer (BCS theory) in 1957 [2] many materials have been discovered which defy this theory. Some materials have transition temperatures that are much higher than can be expected from BCS theory, like for instance the copper oxide high temperature superconductors which were discovered by Bednorz and Müller in 1986 [3]. There are also materials in which superconductivity coexists with magnetic order, even though for a long time it was thought that these two forms of quantum order are incompatible. One of these materials is UCoGe which is the subject of this thesis.

In a ferromagnet below the Curie temperature T_C the spins align parallel to each other to form a net magnetisation. In a standard superconductor Cooper pairs are formed between electrons with opposite spins. Therefore one would expect that these two phenomena exclude each other. For most superconductors this is indeed the case. When magnetic impurities are introduced into a normal superconductor the local field surrounding the impurities suppresses the formation of Cooper pairs and the superconducting transition temperature T_{sc} decreases rapidly as a function of doping. An example of this is shown in figure 1.1 where the superconducting and ferromagnetic transition temperatures of lanthanum doped with gadolinium are plotted versus doping concentration. Lanthanum is a type I superconductor with $T_{sc} = 5.7$ K, whereas gadolinium is a ferromagnet below room temperature ($T_C = 292$ K). T_{sc} of lanthanum strongly decreases with doping and a ferromagnetic phase is induced above three percent of gadolinium doping.

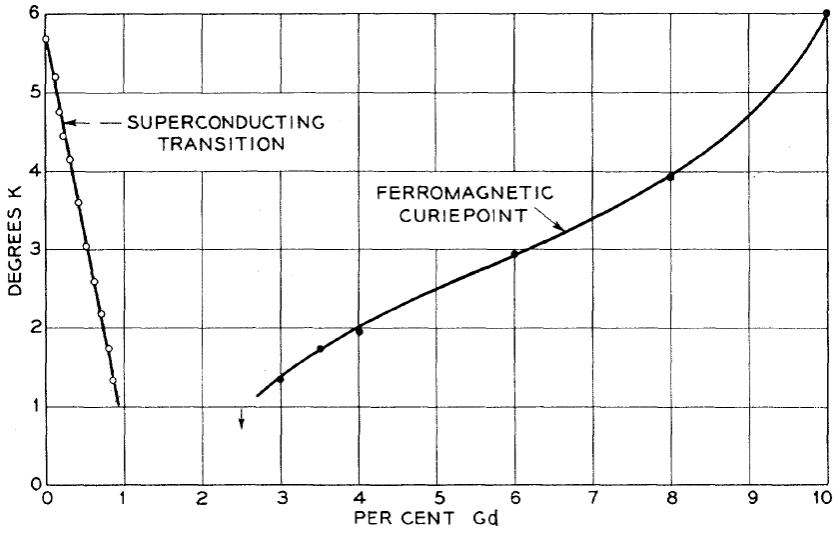

Figure 1.1: *Superconducting and ferromagnetic transition temperatures as a function of doping concentration for lanthanum doped with gadolinium. Taken from Ref. [4].*

There are also materials in which superconductivity and ferromagnetism compete. The so-called Chevrel

phases [5] (for instance $ErRh_4B_4$) and borocarbides [6] are well known examples of this. In these materials $T_{sc} > T_C$, which causes the material to become superconducting at T_{sc} and when the temperature is lowered to T_C superconductivity is destroyed again. This is illustrated for $ErRh_4B_4$ in figure 1.2.

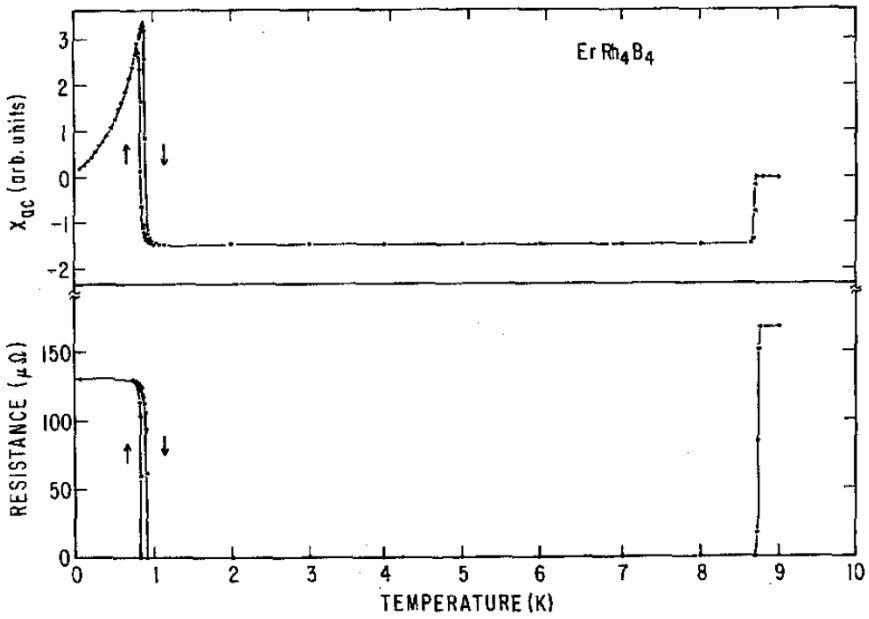

Figure 1.2: *Typical AC-susceptibility χ_{AC} and electrical resistance versus temperature data for $ErRh_4B_4$. Superconductivity sets in below 9 K. When the material is cooled below 1 K superconductivity is destroyed by magnetic ordering. Thermal hysteresis is evident in both properties. Taken from Ref. [7].*

Around 1980 it was recognised that superconductivity could coexist with antiferromagnetic order, where neighbouring spins order in an anti-parallel way. Because the average exchange interaction is almost zero there is no depairing effect on the Cooper pairs. This is for instance the case in heavy fermion antiferromagnets [8].

In the year 2000 the first superconducting ferromagnet was discovered: UGe_2 [9], a material in which superconductivity and ferromagnetism coexist rather than compete. In this material T_{sc} lies well below T_C but superconductivity does not expel magnetism. There is no competition between the two. By now four superconducting ferromagnets have been discovered: UGe_2, UIr [10], URhGe [11] and UCoGe [12]. Some of their properties are listed in table 1.1.

These materials have in common that the magnetic moment is due to the uranium $5f$ electrons and that ferromagnetic order has a strong itinerant character. Another important point is that the same set of electrons is responsible for superconductivity as well as magnetism. All four materials have a low symmetry structure, orthorhombic or monoclinic, which results in strong anisotropy of the electronic and magnetic properties of the material. According to spin fluctuation models for itinerant ferromagnets su-

Material	Structure	T_C (K)	T_{sc} (K)	m_0 (μ_B/U atom)
UGe_2	orthorhombic	53	0.8 ($p = 12$ kbar)	1.5 $\parallel a$
URhGe	orthorhombic	9.5	0.25	0.42 $\parallel c$
UIr	monoclinic	46	0.1 ($p = 27$ kbar)	0.5 $\parallel [1, 0, -1]$
UCoGe	orthorhombic	3	0.6	0.07 $\parallel c$

Table 1.1: *Some characteristic properties of ferromagnetic superconductors. Crystal structure, Curie temperature T_C, superconducting transition temperature T_{sc} and ordered moment m_0.*

perconductivity occurs close to the ferromagnetic quantum critical point where critical spin fluctuations mediate the pairing of electrons in triplet Cooper pairs [13]. This is to be contested with phonons that mediate singlet superconductivity in BCS superconductors.

At ambient pressure UGe_2 and UIr do not have a superconducting phase. Superconductivity is pressure induced for these materials. For UGe_2 magnetic order enters at ambient pressure at $T_C = 53$ K and is gradually suppressed with pressure. It vanishes via a first order transition at a critical pressure of 16 kbar. The pressure temperature phase diagram is shown in figure 1.3. Superconductivity appears at 10 kbar and has a maximum T_{sc} of 0.8 K near 12 kbar. Superconductivity disappears together with magnetism at 16 kbar. An additional first order phase transition exists between a high-temperature-low-moment ($\sim$ 1 μ_B) phase FM1 and a low-temperature-high-moment ($\sim$ 1.5 μ_B) phase FM2. This phase line ends at the maximum of T_{sc}.

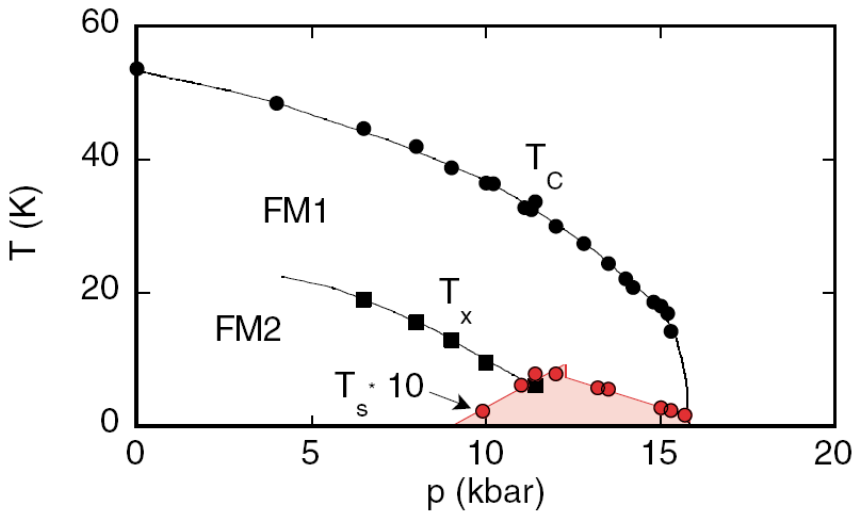

Figure 1.3: *Phase diagram of UGe_2 determined by magnetisation measurements under pressure. T_C is the Curie temperature and T_x locates the phase transition between two ferromagnetic phases FM1 and FM2 with different polarisations. The pressure variation of the superconducting transition temperature T_{sc} ($\times 10$) is determined by electrical resistivity measurements. Taken from Ref. [14].*

For UIr the situation is similar, but not the same. In this material there are three different ferromagnetic phases and superconductivity appears in the third one. The pressure temperature pressure phase diagram is shown in figure 1.4. At ambient pressure $T_C = 46$ K. The first magnetic phase FM1 with an ordered moment of 0.5 μ_B per uranium atom disappears at a critical pressure of 17 kbar. FM2 has a smaller ordered moment of 0.08 μ_B per uranium atom, this phase disappears at a critical pressure of 21 kbar. The third phase in which superconductivity appears has an ordered moment of 0.07 μ_B per uranium atom and vanishes together with superconductivity at a pressure of 28 kbar via a second order phase transition. Neither UGe_2 nor UIr has a superconducting phase in the paramagnetic region of the phase diagram.

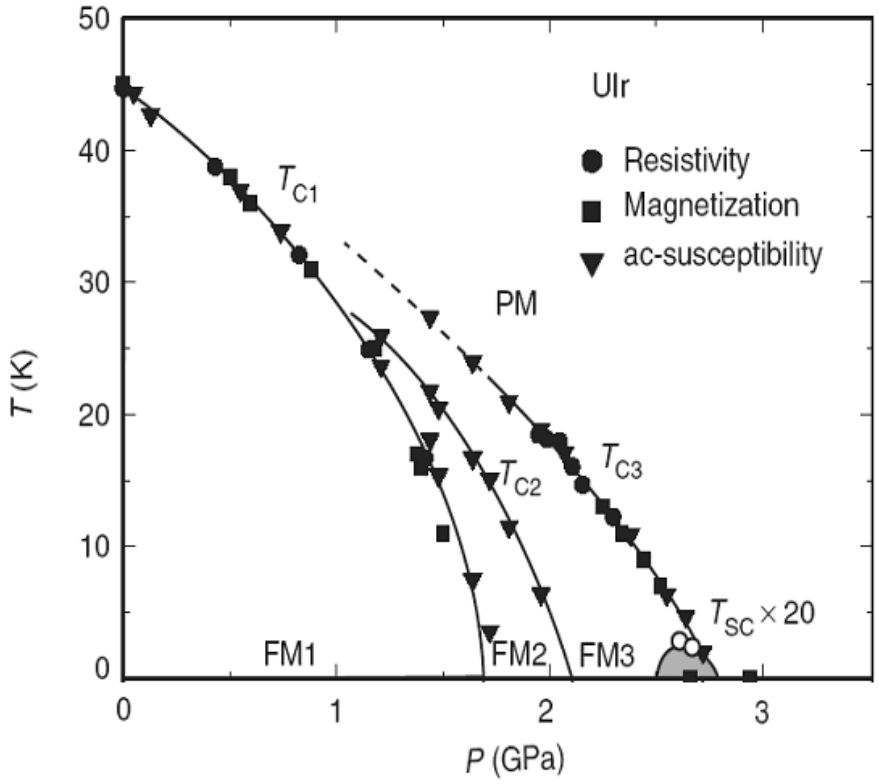

Figure 1.4: *Phase diagram of UIr determined by resistivity, magnetisation and AC-susceptibility measurements under pressure. Three ferromagnetic phases FM1-3 are found. Superconductivity at T_{sc} ($\times 20$) occurs in the FM3 phase near the ferromagnetic quantum critical point. Adapted from Ref. [15].*

The situation in URhGe is completely different. Aplying pressure does not drive the system towards the quantum critical point, but rather away from it. Unlike UGe_2 and UIr this is an ambient pressure ferromagnetic superconductor. The pressure temperature phase diagram is shown in figure 1.5. Magnetism sets in at a temperature of 9.5 K and the ordered moment is 0.42 μ_B per uranium atom. Superconductivity appears at $T_{sc} = 0.25$ K. When pressure is applied T_C increases at a rate of 0.065 K/kbar up to the

highest pressure measured (130 kbar). Superconductivity is depressed with pressure and vanishes near 30 kbar.

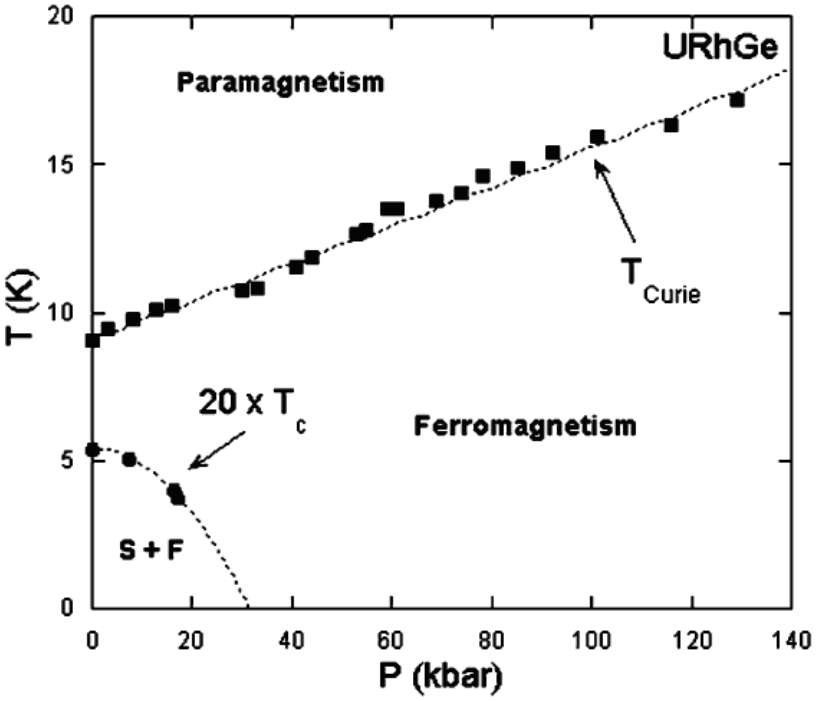

Figure 1.5: *Phase diagram of URhGe. The Curie temperature as determined by ac-calorimetry. Ferromagnetism is present up to pressures of 1.3 GPa. The superconducting transition temperature T_{sc} ($\times 20$) is determined by electrical resistivity. Taken from Ref. [16].*

In this thesis we will present the pressure temperature phase diagram of the fourth ferromagnetic superconductor UCoGe which was discovered by Huy *et al.* in 2006 [12]. Like URhGe, UCoGe is an ambient pressure ferromagnetic superconductor. A typical resistivity curve showing both the ferromagnetic and superconducting transition is shown in figure 1.6. Weak itinerant ferromagnetic order sets in at a temperature of 3 K and superconductivity sets in at a temperature of 0.6 K. It has a low symmetry orthorhombic structure and a small ordered moment of 0.07 μ_B per uranium atom which is directed along the crystallographic c-axis as shown in figure 1.7. The dotted line represents a fit to the relation $m(T^2) = m_0^2(1 - (T/T^*)^2)$, which is predicted for weak itinerant ferromagnets [17], with $T^* \sim T_C$ and the ordered moment $m_0 = 0.07$ μ_B/f.u. In Ref [18] unambiguous proof is given by muon-spin relaxation measurements that weak magnetism is a bulk property which coexists with superconductivity at temperatures below 1 K.

A prediction of the pressure dependence of T_C and T_{sc} can be made using the Ehrenfest relations for second-order phase transitions. This requires data from specific heat and thermal expansion experi-

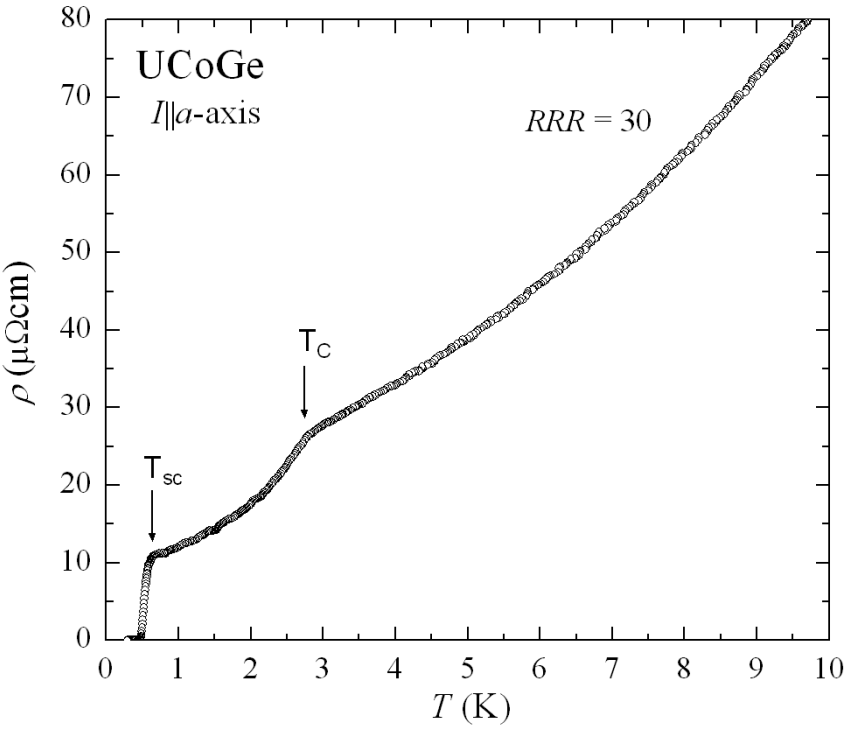

Figure 1.6: *Temperature variation of the resistivity of annealed single crystalline UCoGe for a current $I \parallel a$. Arrows indicate the Curie temperature $T_C = 2.8$ K and the onset temperature for the superconducting transition $T_{sc,onset} = 0.6$ K. Taken from Ref. [19].*

ments. The data have been reported in Ref. [12] and yield the following rates of change in T_C and T_{sc}: $dT_C/dp = -0.25$ K/kbar and $dT_{sc}/dp = 0.02$ K/kbar. These values suggest a relatively low critical pressure $p_c = 12$ kbar at which magnetism would disappear. This pressure is easily accessible using modern experimental techniques, allowing us to investigate the pressure temperature phase diagram of UCoGe. In the following chapter (Theoretical aspects) an overview will be given of the theoretical background of this thesis. This includes a short summary of theories concerning the coexistence of superconductivity and magnetism, a discussion of the symmetry groups and the nature of the different phases of UCoGe and finally we discuss the upper critical field. In Chapter three we will describe the experiments carried out in order to study UCoGe. The experimental results will be presented and discussed in chapter four and all conclusions will be summarised in chapter five.

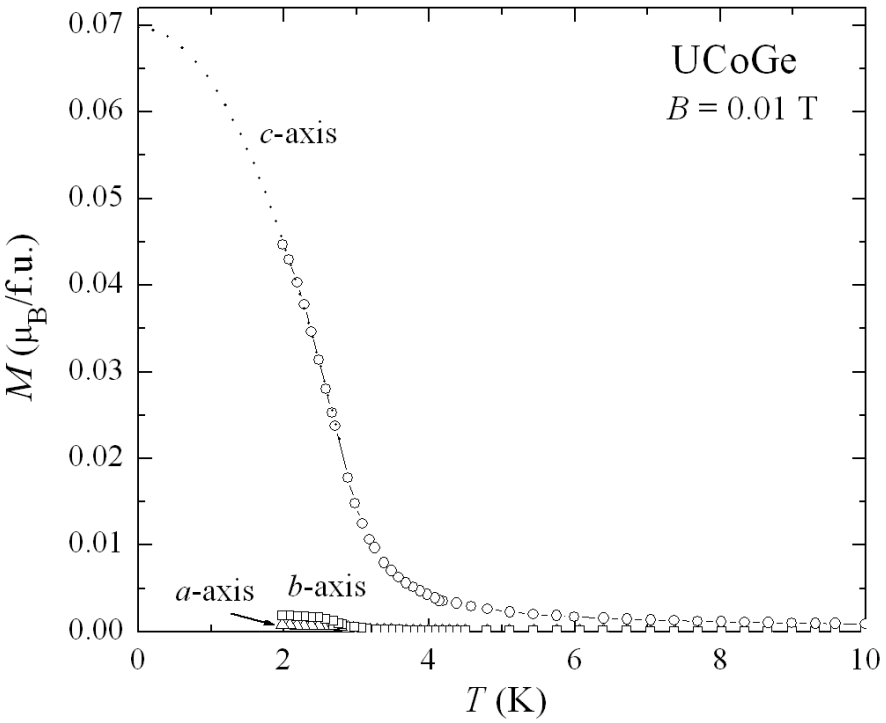

Figure 1.7: *Temperature dependence of the magnetisation of single crystalline UCoGe measured in a field of 0.01 T applied along the principal axes as indicated. The dotted line represents a fit to the relation* $m(T^2) = m_0^2(1 - (T/T^*)^2)$ *(see text). Taken from Ref. [19].*

2 Theoretical aspects

In this chapter an overview is given of the theoretical aspects relevant to this thesis. First we deal with theoretical ideas about the coexistence of superconductivity and magnetism. Then we will present the symmetry groups which have been derived for an orthorhombic ferromagnetic superconductor. We will conclude with a discussion about the upper critical field.

2.1 Superconductivity and magnetism

As described in chapter 1 the coexistence of superconductivity and ferromagnetism is a very peculiar and counter intuitive phenomenon. In a normal superconductor Cooper pairs are formed by electrons with opposite spins and the attractive interaction between the electrons is mediated by phonons. The spin wave function of such a singlet Cooper pair is given by

$$\phi_s = \frac{1}{\sqrt{2}}(|\uparrow\downarrow\rangle - |\downarrow\uparrow\rangle) \tag{2.1}$$

This state has a total spin $S = 0$ and can be of s-wave ($L = 0$) or d-wave ($L = 2$) symmetry. A ferromagnetic superconductor is (most likely) a triplet superconductor. In such a system the spin wave function can be represented by

$$\phi_t = \begin{cases} |\uparrow\uparrow\rangle \\ \frac{1}{\sqrt{2}}(|\uparrow\downarrow\rangle + |\downarrow\uparrow\rangle) \\ |\downarrow\downarrow\rangle \end{cases} \tag{2.2}$$

Here $S = 1$ and the symmetry is p-wave ($L = 1$) or f-wave ($L = 3$). The first and third relations in equation 2.2 are so-called equal spin pairing states. In a ferromagnetic superconductor the spin up and spin down bands are split by the exchange interaction and it is usually assumed that the energy splitting is so large that there is no coupling between the spin up and spin down band and only equal spin pairing states are formed. The mechanism which mediates the interaction is unknown, there is much evidence however that spin fluctuations provide the superconducting glue. For nearly ferromagnetic systems the effective spin coupling tends to be attractive for electrons of the same spin. At low enough temperatures such an attractive interaction will lead to the formation of Cooper pairs of parallel spins i.e. triplet equal spin pairing states [20].

The superconducting phase is characterised by an order parameter which is usually the superconducting gap function $\Delta(\mathbf{k})$. For a BCS superconductor the energy gap has the same symmetry as the Fermi surface and is nearly isotropic. For a triplet superconductor the gap has a lower symmetry than the Fermi surface, which results in strong anisotropic behaviour and line or point nodes appear in $\Delta(\mathbf{k})$.

This indicates a polar or axial state respectively, which has very significant consequences for the upper critical field. We will discuss this in more detail in section 2.3. The shapes of $\Delta(\mathbf{k})$ for an s-wave state, a polar state and an axial state are shown in figure 2.1.

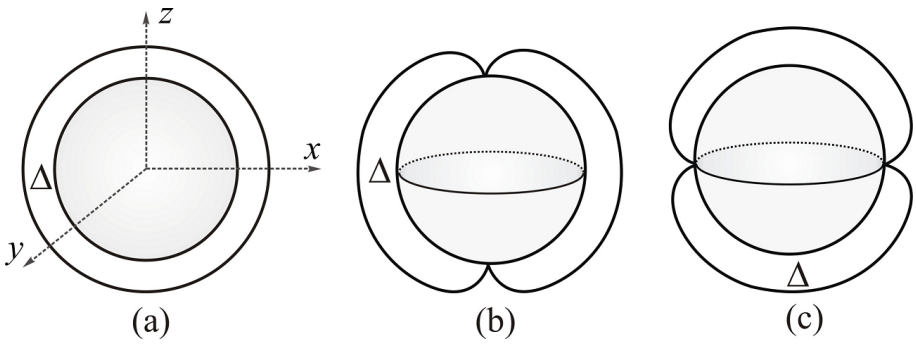

Figure 2.1: *Schematic diagram of the energy gap Δ at the Fermi surface of a superconductor. (a) The isotropic gap of an s-wave superconductor. (b) Axial state with point-nodes. The gap vanishes at two opposite points (poles) on the Fermi surface. (c) Polar state with line-nodes. The gap vanishes at a line (equator) on the Fermi surface.*

Fay and Appel considered the possibility of the coexistence of weak itinerant ferromagnetism and triplet superconductivity [21]. They found that it is very well possible for the two to coexist and that the same electrons responsible for magnetism are also responsible for superconductivity. They were able to calculate the superconducting transition temperature for both the spin up and spin down band as a function of the Stoner parameter. This is shown in figure 2.2.

In this model superconductivity is destroyed right at the transition from the paramagnetic ($I < 1$) to the ferromagnetic ($I > 1$) phase, the ferromagnetic quantum critical point. The critical temperatures for the spin up and spin down band are not the same. Upon lowering the temperature first the spin up electrons pair and when the temperature is lowered even further spin down electrons pair. Experimentally a transition into a second superconducting phase has never been observed. A possible explanation for this is that T_{sc} is much higher in the ferromagnetic phase, because of magnons coupling to the longitudinal susceptibility. This enhances T_{sc} to experimentally accessible values [22]. The Stoner parameter can be changed by means of a control parameter such as a magnetic field, doping or applying pressure. This model leads to the generic phase diagram shown in figure 2.3.

The second superconducting phase outside of the magnetic phase has never been observed experimentally (see chapter 1). In this thesis it will be shown that under high pressure UCoGe does exhibit a superconducting phase in the paramagnetic phase, however T_{sc} is not zero at the critical point like in the generic phase diagram. In fact it has a maximum at the pressure where T_C becomes lower than T_{sc}, we will call this pressure p^*.

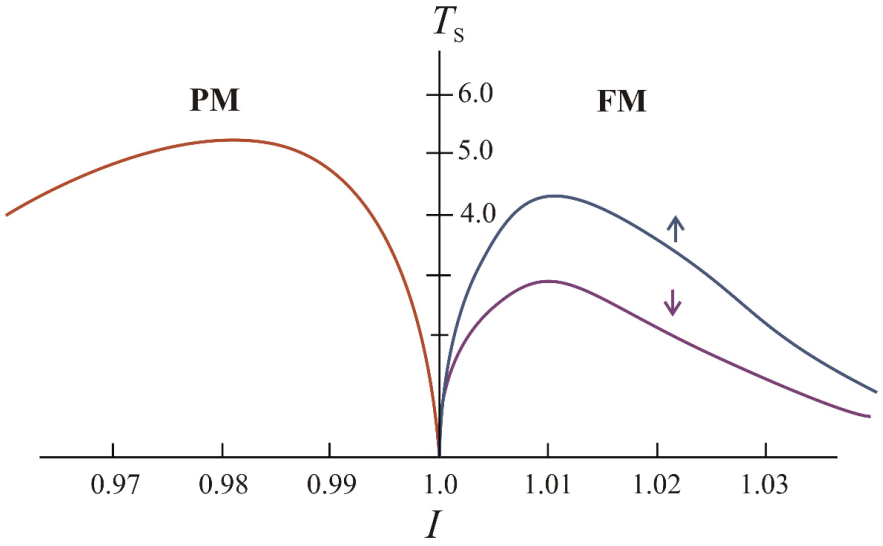

Figure 2.2: *The superconducting transition temperature as a function of the exchange parameter I. Taken from Ref. [21]. The arrows indicate the superconducting transition for the spin up* (↑) *and spin down* (↓) *bands. Superconductivity is destroyed at the transition from the paramagnetic (PM) to the ferromagnetic (FM) phase.*

2.2 Symmetry considerations

As mentioned in the previous paragraph superconductivity in UCoGe persists outside of the magnetic region in the phase diagram. T_C decreases gradually and intersects with T_{sc} at p^*. The magnetic transition vanishes at the ferromagnetic quantum critical point at the critical pressure p_c. A sketch of the pressure temperature phase diagram in which all phases are indicated is given in figure 2.4. In order to understand the nature of the different phases we must first analyse the symmetry groups of each phase. In the paramagnetic (PM) phase the symmetry is determined by elements of the group

$$G_{PM} = D_2 \times U(1) \times T \tag{2.3}$$

Where $D_2 = (E, C_2^x, C_2^y, C_2^z)$ is the point symmetry group of the orthorhombic lattice including operations C_2^x, C_2^y and C_2^z which represent rotation of an angle π around the x, y and z axes respectively. $U(1)$ is the group of gauge symmetry transformations and T is the time reversal operation.

At ambient pressure, when the temperature is lowered the system first enters a ferromagnetic (FM) phase. This causes a magnetic moment along one of the crystallographic axes to appear. We will choose this axis as the z-axis. Performing the time reversal operation results in reversing the direction of the

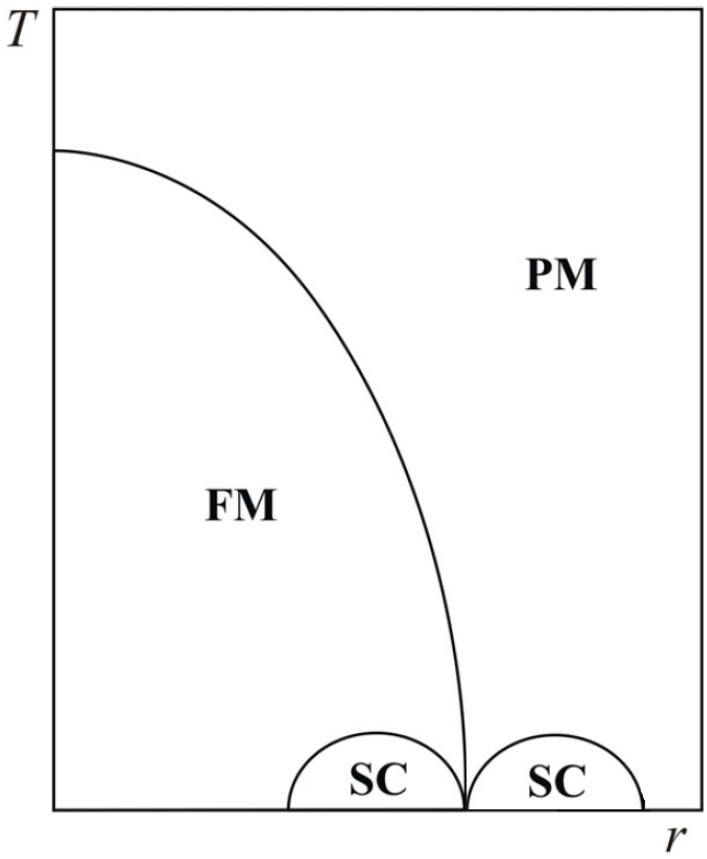

Figure 2.3: *The generic phase diagram for a ferromagnetic superconductor. The transition temperatures are plotted as a function of a control parameter r. Two superconducting (SC) phases appear on the left and right hand side of a ferromagnetic quantum critical point. Superconductivity and ferromagnetism (FM) coexist. The superconducing phase in the paramagnetic (PM) region has never been observed.*

magnetic moment. When no moment is present this is a perfectly valid operation, in the ferromagnetic phase there is a magnetic moment and then time reversal is not a valid operation. The ferromagnetic phase breaks time reversal symmetry. This leads to the following symmetry group for the FM phase

$$G_{FM} = D_2(C_2^z) \times U(1) \tag{2.4}$$

Where

$$D_2(C_2^z) = (E, TC_2^x, TC_2^y, C_2^z) \tag{2.5}$$

represents the magnetic class or the point symmetry group of a ferromagnet. Performing the rotation operation C_2^x or C_2^y has no effect on the crystal structure, but it does reverse the magnetic moment. Therefore it needs to be accompanied by the time reversal operation in order to keep the orientation

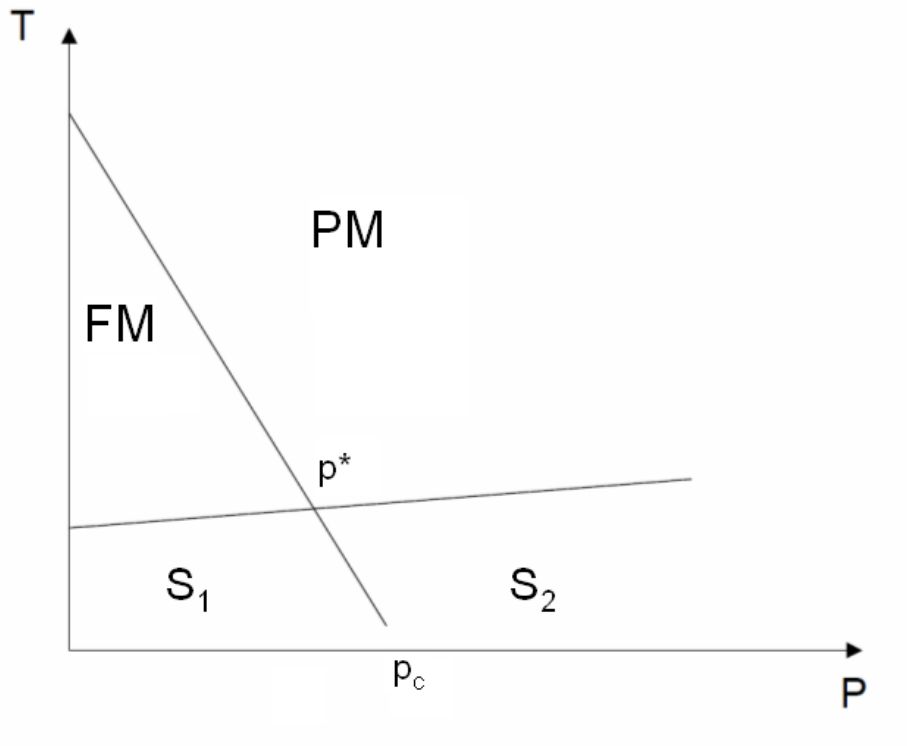

Figure 2.4: *A sketch of the pressure temperature phase diagram of UCoGe taken from Ref. [23]. The superconducting and magnetic phase lines intersect at p^*. The pressure at which $T_C = 0$ is the critical pressure p_c. PM is the paramagnetic phase, FM is the ferromagnetic phase, S_1 is the ferromagnetic superconducting phase and S_2 is the superconducting phase in the paramagnetic region.*

of the magnetic moment constant. Lowering the temperature even further brings the system into the ferromagnetic superconducting phase (S_1). A key signature of superconductivity is that it breaks gauge symmetry, which means that the phase of the wave function becomes equal for the entire superconductor. This leads to this symmetry group for S_1

$$G_{S_1} = D_2(C_2^z) \tag{2.6}$$

Now we take equation 2.3 as a starting point again but we move to a higher pressure, such that there is no ferromagnetic phase between the paramagnetic and the superconducting phase. In other words we move to a pressure $p > p_c$. Upon lowering the temperature the system enters a conventional superconducting phase S_2 and once again gauge symmetry is broken. This leads to the following symmetry class

$$G_{S_2} = (E, C_2^x, C_2^y, C_2^z) \times T \tag{2.7}$$

G_{S_1} is a subgroup of both G_{S_2} and G_F, which means it can be created smoothly from both phases. Because of this all phase transitions in the phase diagram are second order transitions [23].

In Ref [23] Mineev also gives a general form of the order parameter for a two-band itinerant ferromagnetic superconductor with orthorhombic crystal symmetry. Ferromagnetic order is assumed to be uniaxial with the ordered moment m_0 pointing along the z direction, spin orbit coupling is assumed to be strong. Equal spin pairing states formed by spin up electrons from one band and spin down electrons from another give rise to a two component order parameter.

$$\begin{aligned} \mathbf{d}_1(\mathbf{k}) &= \Delta_\uparrow(\mathbf{k})(\hat{x} + i\hat{y}) \\ \mathbf{d}_2(\mathbf{k}) &= \Delta_\downarrow(\mathbf{k})(\hat{x} - i\hat{y}) \end{aligned} \tag{2.8}$$

Here $\hat{x}$ and $\hat{y}$ are unit vectors of the spin coordinate system pinned to the crystal axes.

There are two different co-representations for the ferromagnetic superconducting state: A and B. All states relating to a given co-representation have the same critical temperature. The order parameter amplitudes for states A and B are given by

$$\begin{aligned} \Delta^A_\uparrow(\mathbf{k}) &= \eta_1(k_x u_1 + i k_y u_2) \\ \Delta^A_\downarrow(\mathbf{k}) &= \eta_2(k_x u_3 + i k_y u_4) \end{aligned} \tag{2.9}$$

$$\begin{aligned} \Delta^B_\uparrow(\mathbf{k}) &= \eta_1(k_z v_1 + i k_x k_y k_z v_2) \\ \Delta^B_\downarrow(\mathbf{k}) &= \eta_2(k_z v_3 + i k_x k_y k_z v_4) \end{aligned} \tag{2.10}$$

Where the functions $u_i = u_i(k_x^2, k_y^2, k_z^2)$ and $v_i = v_i(k_x^2, k_y^2, k_z^2)$ are invariant with respect to all transformations of the orthorhombic symmetry group.

Neighbouring domains with opposite direction of magnetisation are occupied by the time reversed states A^* and B^* which are characterised by the complex conjugate order parameter. For the A^* phase this is given by

$$\begin{aligned} \mathbf{d}^*_1(\mathbf{k}) &= \zeta_1(k_x u_1 - i k_y u_2)(\hat{x} + i\hat{y}) \\ \mathbf{d}^*_2(\mathbf{k}) &= \zeta_2(k_x u_3 - i k_y u_4)(\hat{x} - i\hat{y}) \end{aligned} \tag{2.11}$$

A similar expression can be written down for B^* The superconducting gap functions of A and B have axial and polar symmetry respectively, see figure 2.1. The consequences of the symmetry of the superconducting gap function will be discussed in section 2.3.

Having identified the symmetry classes and order parameters of the different phases we will now proceed with the nature of the phases. The triplet superconducting phases of UCoGe are comparable to those of superfluid ^{3}He. For the definitions of all phases of superfluid ^{3}He see for instance Ref. [24]. The S_1 phase is an analogue of the A_2 phase. This is a spin non-polarised phase consisting of spin up and

down equal spin pairing states. The A_2 phase is a linear combination of two states $|S_z = 1, m = 1\rangle$ and $|S_z = -1, m = 1\rangle$ with almost equal populations.

The energy difference between the spin up and spin down band is maintained by the exchange field. Increasing the pressure, starting in the S_1 phase, lowers the exchange field, which in turn causes the difference between the spin up and down bands to decrease until the two bands become degenerate at the critical pressure p_c and the system enters the S_2 state. This is not necessarily a triplet state like S_1. From symmetry arguments alone we cannot dismiss the possibility of a normal singlet state. If it is a triplet state however, it is similar to the *planar* phase of ^{3}He. This phase is a superposition of two states $|S_z = 1, m = -1\rangle$ and $|S_z = -1, m = 1\rangle$ with equal populations. Unlike the A_2 phase, this phase does not break time reversal symmetry.

Our techniques do not allow us to experimentally tell the difference between the A_2 and the planar phase. But if S_2 is a singlet phase rather than a triplet phase we will be able to tell the difference by measuring the upper critical field.

2.3 Upper critical field

For a normal BCS superconductor an upper boundary is given for the upper critical field by the Pauli paramagnetic limit, which was first calculated in Ref. [25]. In zero magnetic field the spin up and spin down bands of a superconductor are degenerate. Applying a field will lift this degeneracy and favour one band (spin up) over the other (spin down). This is illustrated in figure 2.5. The energy difference between the two bands depends on the magnetic field. Eventually the band splitting will become so large that coupling between the two bands is no longer possible and BCS Cooper pairs can no longer be formed. The Pauli paramagnetic limit is given by

$$B_{c2}^{Pauli} \approx 1.83 \times T_{sc} \tag{2.12}$$

For a superconductor with $T_{sc} \approx 0.7$ K this is approximately equal to 1.3 T. In chapter 4.1 it will be shown that the upper critical field of UCoGe is approximately 5 T at ambient pressure, this is clearly higher than 1.3 T, providing evidence for triplet superconductivity. If the S_2 phase is a singlet superconductor it should obey the Pauli limit and a large drop in the upper critical field should be observed.

The upper critical field as a function of temperature for UCoGe shows a strong anisotropy [26] as shown in chapter 4.1. The upper critical field measured with $B \parallel I \parallel a, b$ is a factor 10 larger than with $B \parallel I \parallel c$. This can be explained by considering the superconducting gap function to which we will turn now.

The order parameter for an orthorhombic ferromagnetic superconductor with spin triplet pairing and

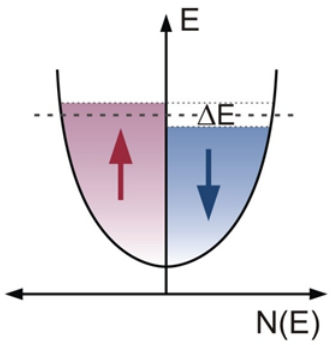

Figure 2.5: *The density of states (N(E)) as a function of energy (E) for a spin up and a spin down band in magnetic field. The bandsplitting (ΔE) depends on the magnetic field. If ΔE is large enough Cooper pairs can no longer be formed. This is called the Pauli paramagnetic limit.*

strong spin-orbit coupling (given in section 2.2) has been worked out by Fomin [27] and Mineev [28] under the assumption of a sufficiently large exchange splitting, such that there is no coupling between electrons from the spin up and spin down band. Symmetry considerations show that only two different symmetries for the superconducting gap function are possible. In the A phase the gap has zeros parallel to the magnetic moment ($k_x = k_y = 0$). In other words, it has axial symmetry with point nodes along the magnetic moment direction m_0. The B phase has a line of zeros on the equator of the Fermi surface ($k_z = 0$). This gap has polar symmetry with a line of nodes perpendicular to m_0. This is shown in figure 2.1. Which of these scenarios is the case can be deduced from the anisotropy of the upper critical field. The effect of an anisotropic p-wave interaction has been investigated by Scharnberg and Klemm [29]. If the p-wave interaction favours one direction over the other two this would lead to a polar state. If, on the other hand, the interaction is weakest in one direction this would lead to an axial state. In the case of a polar state with the maximum gap direction along the uniaxial direction $m_0 \parallel c$, the ratio of upper critical fields perpendicular ($B_{c2}^{\perp}(0)$) and parallel ($B_{c2}^{\parallel}(0)$) to the moment is given by:

$$\frac{B_{c2}^{\perp}(0)}{B_{c2}^{\parallel}(0)} = 0.466\sqrt{\frac{m_{ab}}{m_c}} \tag{2.13}$$

Where m_{ab}/m_c reflects the anisotropy in the effective mass. For the axial state the situation is reversed. The maximum gap direction is perpendicular to the magnetic moment, therefore $B_{c2}^{\perp}(0) > B_{c2}^{\parallel}(0)$. Calculations for $B_{c2}^{\parallel}(0)$ are available in Ref. [30], but $B_{c2}^{\perp}(0)$ has not been calculated yet. In order to determine whether the symmetry of the superconducting gap is polar or axial we will compare these results to experiment in chapter 4.1.

3 Experimental aspects

In this chapter a description is given of the experimental equipment that was used at the Van der Waals-Zeeman Instituut of the University of Amsterdam for the experiments carried out to study UCoGe under high pressure.

3.1 Sample preparation

The samples investigated in this thesis were also used in the work presented in Ref [26]. They were grown by dr. Y.K. Huang in the following way. A polycrystalline batch with nominal composition $U_{1.01}$CoGe was prepared by arc melting the constituents (natural U 3N, Co 3N, and Ge 5N) in a water-cooled copper crucible under a high-purity argon atmosphere. Next, a single-crystalline rod was pulled from the melt using a modified Czochralski technique in a tri-arc furnace under a high-purity argon atmosphere. Electron micro-probe analysis confirmed the single-phase nature of the grown crystal. Single-crystallinity was checked by X-ray Laue backscattering. Samples for various measurements were cut by spark erosion. Transport measurements on the as-grown samples show a residual resistance ratio, (RRR $= \rho(300\,\mathrm{K})/\rho(1\,\mathrm{K}) \approx 5$), and rather poor ferromagnetic and superconducting properties. However, after an annealing procedure, like applied for URhGe [11], the RRR increases to 30, and proper FM and SC transitions appear.

3.2 High pressure experiments

In order to apply pressure to the sample a hybrid piston cylinder pressure cell (shown in figure 3.1) was used. High pressure requires that the cell is made of the strongest material available. This material should also be non-magnetic, otherwise it would interfere with the measurements. The inner cylinder is therefore made of NiCrAl and has a diameter of 6 mm. The sample space has a diameter of 4.7 mm and is 8 mm long. The outer cylinder is made of CuBe and has a diameter of 25 mm. CuBe is not as hard as NiCrAl, but it has a higher plasticity, therefore it is used for the outer cylinder for safety reasons. The cell is 80 mm long. The feedthrough for electrical wiring is made of CuBe. A drawing of the cell is given in figure 3.2.

The cell is pressurised by applying a force using a hand press. The pressure is transferred to the pressure cell via a piston which is made of tungsten carbide. When the pressure is applied the cell is clamped and put in the measurement setup autonomally.

Inside the cell the samples are mounted on a dedicated plug inside a Teflon cylinder. The pressure is transferred to the sample using the hydrostatic pressure transmitting medium Daphne oil 7373. This

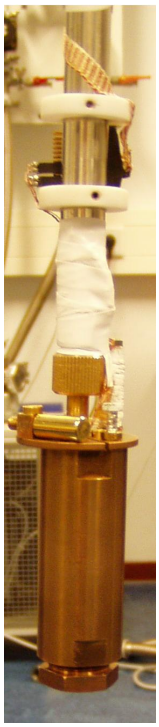

Figure 3.1: *The pressure cell used in these experiments.*

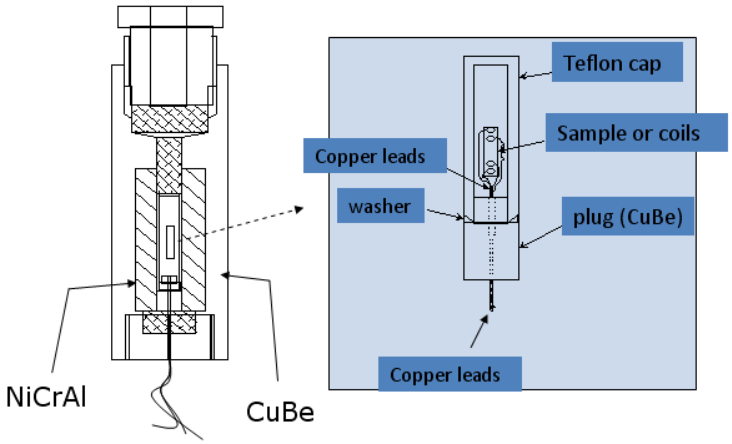

Figure 3.2: *Drawing of the pressure cell, taken from Ref. [31].*

medium solidifies upon cooling which results in a pressure drop of 1.5 kbar irrespective of the initial pressure [32]. Because of this and the fact that it is possible that the pressure may not be transferred optimally (due to for instance a slight misalignment of some parts of the pressure cell) we calibrate the pressure cell. This was done during the AC-susceptibility measurements (chapter 3.4) by measuring the superconducting transition temperature T_{Pb} of a piece of lead. The pressure dependence of T_{Pb} [33] is known, so a measured transition temperature at a certain nominal pressure gives the actual pressure. In this way a graph of the actual pressure versus the nominal pressure can be created. We also use this

calibration for the resistivity measurements under pressure (chapter 3.5).

T_{Pb} versus nominal pressure is shown in figure 3.3. It can be seen that the slope of the measured data is not the same as the slope of the literature data. Using the literature data we determine the actual pressure and construct the calibration graph shown in figure 3.4. The slope of the graph gives the pressure efficiency of the pressure cell which is roughly 82 %. The deviation in temperature of each data point from the linear fit is used to determine the horizontal errorbar throughout this thesis.

It can also be seen that the last two data points deviate from the linear behaviour. This indicates a sudden drop in pressure efficiency and it would make further measurements less reliable. This is the reason the experiments were terminated at this point.

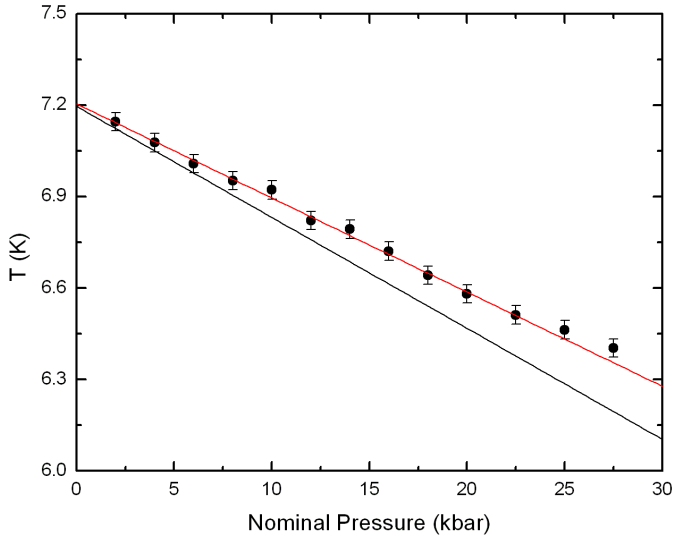

Figure 3.3: *The lead transition temperatures measured by AC-susceptibility versus nominal pressure. The solid red line represents a linear fit to the data. The black line represents literature data from Ref. [33].*

3.3 Heliox

All experiments were done in an Oxford Instruments Heliox VL ^{3}He system, a ^{3}He cryostat with internal adsorption pump. See figure 3.5. The base temperature for this system is 238 mK and the cooling power is 40 μW at 290 mK. Cooling is done by evaporating liquid ^{4}He in the first stage, which cools down the system to approximately 1.5 K, and liquid ^{3}He in the second stage, which cools down the system to base temperature. For more information on helium-3 cryostats, see for instance [34].

The temperature of the system is controlled by an Oxford LabVIEW program and read out by a commercially available RuO_2 thermometer mounted on the sample platform. Inside the cryostat is also a superconducting magnet which can generate fields up to 12 T.

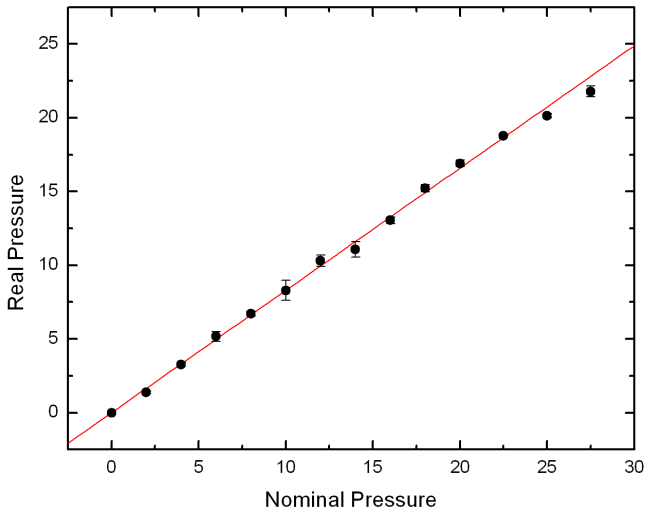

Figure 3.4: *Nominal versus actual pressure. The red line is a linear fit to the data points which gives the pressure cell efficiency.*

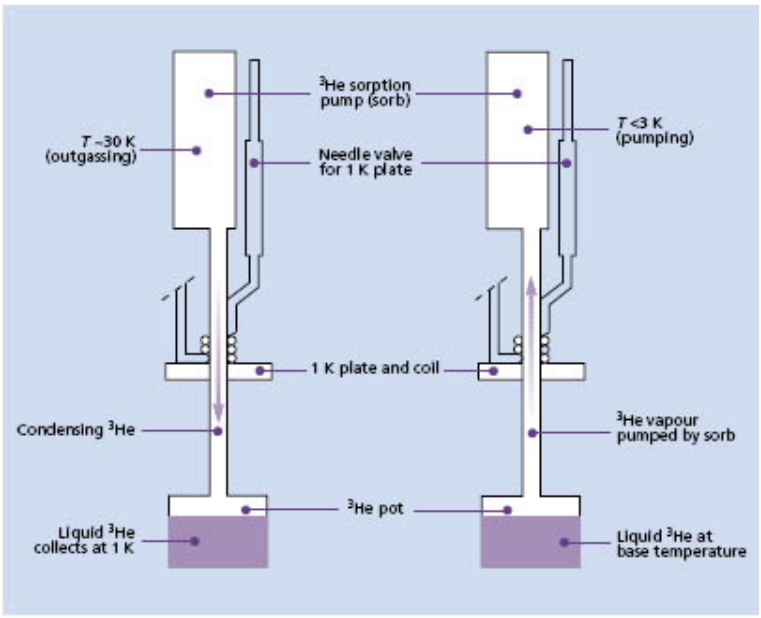

Figure 3.5: *Drawing of the operation principle of the Heliox, taken from [35].*

3.4 AC-susceptibility measurements

AC-susceptibility measurements were done to determine the magnetic and superconducting transition temperatures of a UCoGe single crystal sample, which was cut along the c-axis (RRR $\approx$ 7). The cross section of the sample was approximately 1 mm^2, the length approximately 2 mm. A mutual-inductance

transformer method was applied [36]. The driving field (4.6 μT) is generated in the primary coil, which is 8 mm long and has 100 windings. Inside this coil there are two secondary coils wound in opposite direction (see figure 3.6). For perfectly balanced coils the output signal is zero. The sample is placed in one of the secondary coils and a piece of lead is placed in the other one. As the pressure dependence of the superconducting transition temperature of lead is known, measuring the superconducting transition will yield the pressure inside the pressure cell. So the piece of lead is used as a manometer. The superconducting transition temperature of lead is 7.2 K [33] at ambient pressure and decreases linearly with pressure with a slope of 0.036 K/kbar. In the pressure range investigated all transition temperatures of lead are well away from the ferromagnetic and superconducting transitions of UCoGe, so the lead signal does not interfere with the measurement.

The induced voltage in the secondary coils, which is a direct measure for the susceptibility, is measured with an EG&G Instruments 7260 DSP lock-in amplifier which operates at a frequency of 113 Hz. The measured signal depends linearly on this frequency. Above 10 kbar a lower noise level was needed, therefore the operating frequency was changed from 113 Hz to 313 Hz. The applied excitation current is 300 μA.

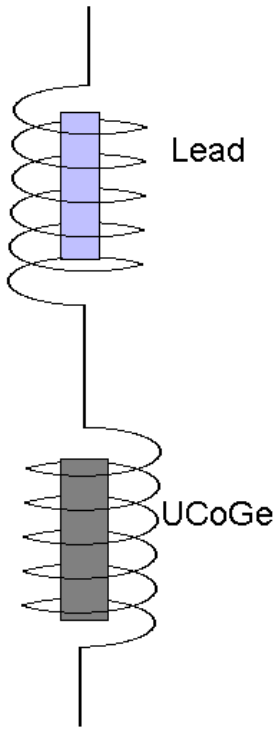

Figure 3.6: *The oppositely wound secondary coils with the UCoGe single crystal sample and the lead manometer in them. These are placed inside a primary coil which generates the AC magnetic field.*

3.5 Resistivity measurements

Resistivity measurements were done on two different UCoGe single crystalline samples. One cut along the a-axis (RRR $\approx$ 27) and one along the c-axis (RRR $\approx$ 7). The c-axis sample is the same one as used in the AC-susceptibility measurements. A standard four-probe low frequency AC-technique was used inside the same pressure cell used in chapter 3.4. A current is passed through the two outer contacts and the voltage drop across the two inner contacts is measured. The contacts are made using thin copper wire (30 μm) and glued to the sample using silver paste. The configuration is shown in figure 3.7 and a picture of the plug inside the pressure cell is shown in figure 3.8.

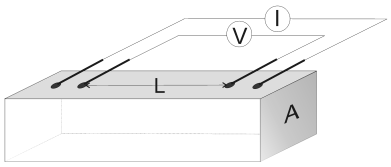

Figure 3.7: *The contact geometry for the resistivity measurements.*

The samples were bar shaped with a cross section A of approximately 1 mm^2, the length of the samples was 4 mm. The distance between the inner contacts L was approximately 2 mm. The resistivity ρ and the resistance R are related to each other by

$$\rho = R\frac{A}{L} \tag{3.1}$$

It is quite difficult to determine the distance between the contacts because of the relatively large spread of the silver paste. Also micro cracks in the samples can give rise to an effective cross section which is larger than the real A. Because of these two reasons the error in the geometrical factor A/L can be in the order of 10% and absolute values of resistivity data should be interpreted with care. In this thesis all resistivity data are normalised to room temperature resistance, cancelling out the geometrical factor. The RRR, which is a measure for the quality of the sample, is not affected by the geometrical factor.
The resistivity data were obtained using a Linear Research AC Bridge Resistance model LR700. A low excitation current of 100 μA was used at a frequency of 16 Hz in order to prevent heating of the sample when measuring at low temperatures.
The pressure inside the pressure cell was determined using the calibration graph (figure 3.4).

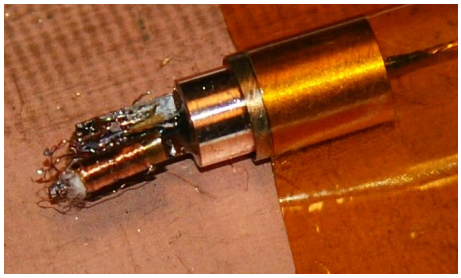

Figure 3.8: *The plug on which the samples are mounted inside the pressure cell during the resistivity measurements.*

3.5.1 Upper critical field measurements

During the resistivity measurements the upper critical field (B_{c2}) of the two single crystal samples has also been measured. This was done by applying a magnetic (DC) field in the heliox using the superconducting magnet. Then the superconducting transition was measured. Due to the magnetic field the transition temperature is depressed. By increasing the magnetic field in small steps and following the transition down to base temperature a B-T phasediagram can be constructed for each pressure. The curves can then be extrapolated to give $B_{c2}(T = 0)$ for each pressure.

4 Experimental results

In this chapter the results will be presented and discussed. We will start by giving an overview of work on UCoGe which has already been reported in the literature and is relevant to this thesis. After that we will proceed with the data acquired from AC-susceptibility and resistivity measurements. The phase diagram which is constructed using this data is discussed next and we end with the critical field measurements.

4.1 Previous work on UCoGe

In this paragraph we will discuss some of the work that has been reported in the literature on UCoGe. We will focus on two articles: Unusual Upper Critical Field of the Ferromagnetic Superconductor UCoGe by Huy et al. (Ref. [26]) and Pressure-Temperature Phase Diagram of Polycrystalline UCoGe Studied by Resistivity Measurements by Hassinger et al. (Ref. [37]).

4.1.1 Upper critical field at ambient pressure

In Ref. [26] the suppression of superconductivity of single crystalline UCoGe was investigated by resistivity measurements in fixed magnetic fields applied along the orthorhombic a and b and c axes. The results are shown in figure 4.1. Three important features should be noted. I) The large value of $B_{c2}(0) \approx 5$T for $B \parallel a, b$. II) The large anisotropy $B^a_{c2} \simeq B^b_{c2} \gg B^c_{c2}$. And III) the pronounced upturn in $B_{c2}(T)$ measured in all three directions.

As explained in chapter 2.3 the large value of $B_{c2}(0)$ is much larger than expected for a BCS singlet superconductor with $T_{sc} \approx 0.7$ K based on the Pauli paramagnetic limit for singlet superconductivity. Therefore the high value of $B_{c2}(0)$ provides evidence for a triplet state with equal spin pairing.

For a orthorhombic uniaxial ferromagnetic superconductor only two symmetries for the superconducting gap function are possible: the axial and the polar state. These structures have been discussed in chapter 2.3 and they are shown in figure 2.1. The gap function can be used to predict the anisotropy in the $B_{c2}(T)$ curves. In figure 4.1 these predictions are compared to the measurements. In a polar state the upper critical field in the direction perpendicular to the magnetic moment would be a factor two smaller than in the direction of the ordered moment (formula 2.13), this is clearly not in agreement with the data. For the axial state the situation is reversed and $B^{\perp}_{c2}(0) > B^{\parallel}_{c2}(0)$, this is in agreement with the data. Calculations for $B^{\parallel}_{c2}(T)$ are available for the axial state in Ref. [30], unfortunately calculations for $B^{\perp}_{c2}(T)$ are not. The gap is maximum however in this direction, therefore the experimental data for B^a_{c2} and B^b_{c2} are compared to the upper critical field for the polar state along the maximum gap direction,

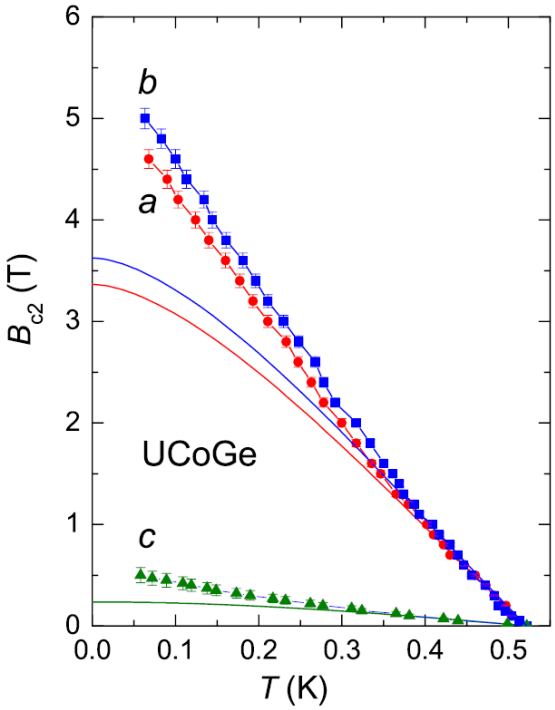

Figure 4.1: *The upper critical field versus temperature for $B \parallel a$, b and c at ambient pressure taken from Ref. [26]. The solid lines show the calculated dependence for a superconducting gap function with axial (along c) and polar (along a and b) symmetries (see text).*

which is very similar to $B_{c2}^{\perp}(T)$ for the axial state. We conclude that the anisotropy in the upper critical field supports an axial state, but the theoretical predictions do not track the data down to the lowest temperatures. This is due to the upward curvature in the $B_{c2}(T)$ curves which is observed for all three directions.

An upward curvature caused by a crossover between two superconducting phases has been predicted by Mineev and Champel [38] for a cubic two-band ferromagnetic superconductor. Evaluation of the linearised Ginzburg-Landau equations including gradient terms showed such an upturn, depending on the strength of the pairing interactions and a number of anisotropy coefficients. Such a crossover is also possible for an orthorhombic system, but calculations for this scenario are not available. Note that the crossover between two phases is field induced and that in zero field only one superconducting transition is predicted.

For a two band superconductor upward curvature in $B_{c2}(T)$ could also naturally be attributed to a field induced redistribution of the states $|\uparrow\uparrow\rangle$ and $|\downarrow\downarrow\rangle$ [38]

4.1.2 Pressure temperature phase diagram of polycrystalline UCoGe

The pressure temperature phase diagram of UCoGe has been studied for a polycrystal in Ref. [37]. The phase diagram obtained in these experiments is shown in figure 4.2. There are two important features in this phase diagram. I) Superconductivity persists throughout the entire pressure range and T_{sc} does not vary strongly as a function of pressure. II) Magnetism can no longer be observed above 8 kbar.

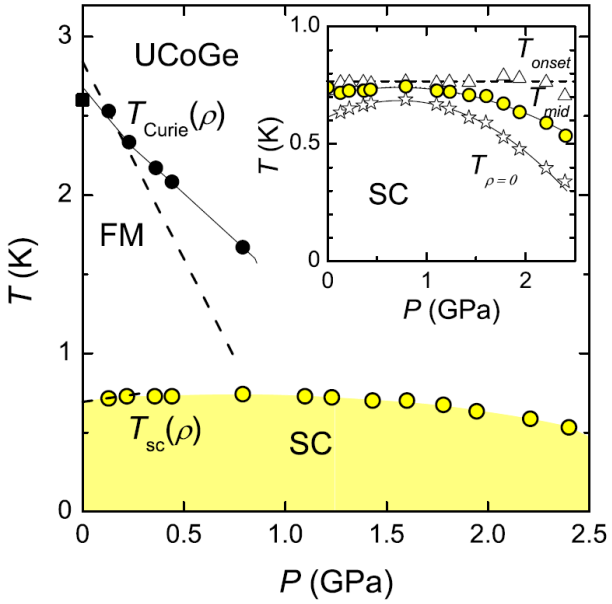

Figure 4.2: *The pressure temperature phase diagram obtained by resistivity measurements from a polycrystal. Taken from Ref. [37]. The black and yellow circles represent T_C and T_{sc} respectively. At zero pressure T_C is determined by AC-susceptibility (full square). The dashed lines indicate the slopes of the transition lines calculated from the Ehrenfest relation at ambient pressure. In the inset the onset-, midpoint-, and zero-resistivity temperatures of the superconducting transition are shown. Lines are guides to the eye.*

Superconductivity persists up to the highest measured pressure of 24 kbar. The fact that superconductivity exists outside of the magnetic phase is truly unique. No other ferromagnetic superconductor shows this kind of behaviour. As mentioned in chapter 1 a superconducting phase outside of the magnetic phase has never been measured for any other ferromagnetic superconductor.

Magnetism is suppressed at a rate of 0.14 K/kbar and the highest pressure at which a magnetic transition could be distinguished was 8 kbar ($T_C \approx 1.6$ K). Due to the broadness of the magnetic transition T_C could no longer be defined above this pressure. T_{sc} first increases as a function of pressure until a maximum of 0.75 K is reached at a pressure of 8 kbar. After this T_{sc} steadily decreases with pressure down to ~ 0.5 K at 2.4 kbar.

In figure 4.3 the results of a $\rho = \rho_0 + A_x T^x$ fit on the resistivity curves as well as the width of the superconducting transition are shown. The absolute value of the resistivity is normalised to $\rho_{RT} = 300\mu\Omega cm$ at room temperature. The value of ρ_{RT} was estimated from the resistivity of a singlecrystalline sample. Therefore the absolute values of ρ_0 and A_x should be interpreted with care. A clear anomaly in all four quantities is visible at a pressure of 8 kbar. The authors refer to this pressure as p^*.

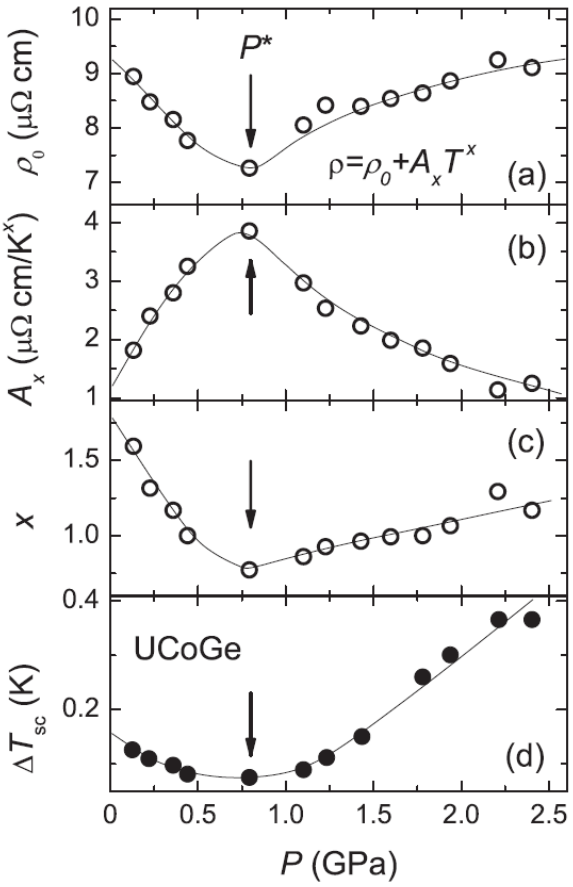

Figure 4.3: *(a)-(c) Pressure dependence of the fit parameters of a $\rho = \rho_0 + A_x T^x$ fit taken from Ref. [37]. The clear anomaly at $p^* \sim 0.8$ GPa (8 kbar) reflects the pressure where the magnetic transition disappears. It corresponds to the pressure where the superconducting transition width ΔT_{sc} is narrowest (d). The lines are guides to the eye.*

For an itinerant ferromagnet close to a magnetic critical point we expect $\rho \propto T^2$ in the ferromagnetic phase due to scattering at magnons and $\rho \propto T^{5/3}$ in the paramagnetic phase due to scattering at critical ferromagnetic spin fluctuations. The difficulty to recover this behaviour has been established for many systems, notably for MnSi [39] and $ZrZn_2$ [40]. We will compare these results with our data in chapter 4.4.

4.2 AC-susceptibility

The AC-susceptibility measurements were done on a single crystalline sample cut along the c-axis (RRR ≈ 7). The results of the AC-susceptibility measurements at all pressures are presented in figure 4.4. As the signal depends linearly on the measurement frequency and different frequencies were used for the low and high pressure measurements each data set has been divided by its measurement frequency and subsequently offset along the vertical axis for clarity. The pressures, ranging from 1.4 kbar (top curve) to 21.8 kbar (inset), are indicated. The pressures in the inset are from right to left: 13.0, 15.2, 16.9, 18.8, 20.1, and 21.8 kbar. From 10.3 kbar on the measurement frequency was increased from 113 Hz to 313 Hz in order to reduce noise. The peak in the measurements (indicated by the arrows) is caused by the magnetic transition. The center of this peak is taken as T_C. It can be seen that the height of this peak steadily decreases and that the peak becomes broader with increasing pressure. The amplitude of the peak versus pressure is plotted in figure 4.14. The highest pressure at which the peak can still be identified is 10.3 kbar. At 11.1 kbar some structure can still be seen just before the superconducting transition, which suggests $T_C \approx T_{sc}$, but no complete magnetic transition is observed. No indication of magnetism was observed for higher pressures.

The diamagnetic signal below 1 K is caused by superconductivity. The midpoint of the transition is taken as T_{sc}. The difference in temperature between the points at which the signal has dropped to 90 and 10% respectively of the paramagnetic state value is taken as an estimate for the width of the superconducting transition. T_{sc} steadily increases up to 11.1 kbar where it achieves its maximum of 604 mK. From that point on it starts decreasing to 288 mK for the highest measured pressure. The magnitude of the diamagnetic signal does not vary with pressure, which confirms bulk superconductivity for the whole pressure range.

4.3 Resistivity

Resistivity measurements were done on two single crystalline samples. One cut along the a-axis (RRR ≈ 27) and one along the c-axis (RRR ≈ 8). The current was applied along the long axis. The results of the measurements on both samples are shown in figures 4.5 ($I \parallel a$) and 4.6 ($I \parallel c$). The data have been normalised to one at room temperature and have subsequently been offset along the vertical axis for clarity. The pressures, ranging from 0.8 to 16.6 kbar are indicated. Magnetism is observed as a kink in the resistivity curve. The kink (indicated by arrows) is taken as T_C. Magnetism can be detected up to 9.5 kbar.

The superconducting transition temperature for $I \parallel a$ ($I \parallel c$) increases steadily from 502 mK (532 mK) at

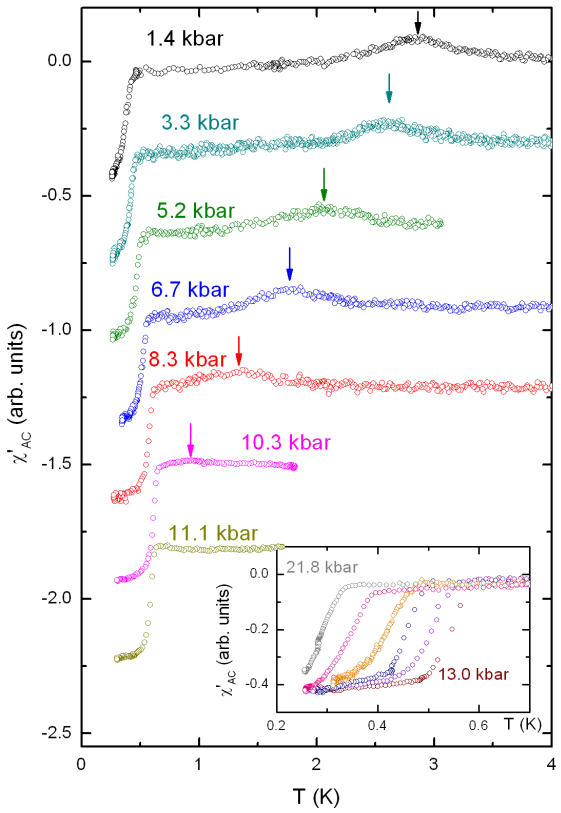

Figure 4.4: *AC-susceptibility versus temperature measured taken at different pressures. The pressures in the inset are from right to left: 13.0, 15.2, 16.9, 18.8, 20.1 and 21.8 kbar.*

0.8 kbar to 747 mK (669 mK) at 9.5 kbar. At higher pressures T_{sc} decreases again down to 657 mK (535 mK) at 16.6 kbar. Also the width of the transition decreases with pressure down to a minimum of 0.02 K (0.03 K) at 9.5 kbar after which the transition becomes broader again. The midpoint of the transition is taken as T_{sc}. The difference in temperature between the points at which the signal has dropped to 90 and 10% respectively of the paramagnetic state value is taken as an estimate for the width of the superconducting transition.

For an itinerant ferromagnet close to a magnetic critical point we expect $\rho \propto T^2$ in the ferromagnetic phase due to scattering at magnons and $\rho \propto T^{5/3}$ in the paramagnetic phase due to scattering at critical ferromagnetic spin fluctuations. The resistivity curves were plotted versus T^x for various values of x, in order to make an estimate of the pressure dependence of this parameter. The value of x at which the curve showed linear behaviour is taken as the exponent. This was done for both the ferromagnetic and paramagnetic phase. An example of this procedure at 3.3 kbar is shown in figure 4.7. The results are shown in figure 4.8. Triangles pointing up represent data measured for $I \parallel a$ and triangles pointing down

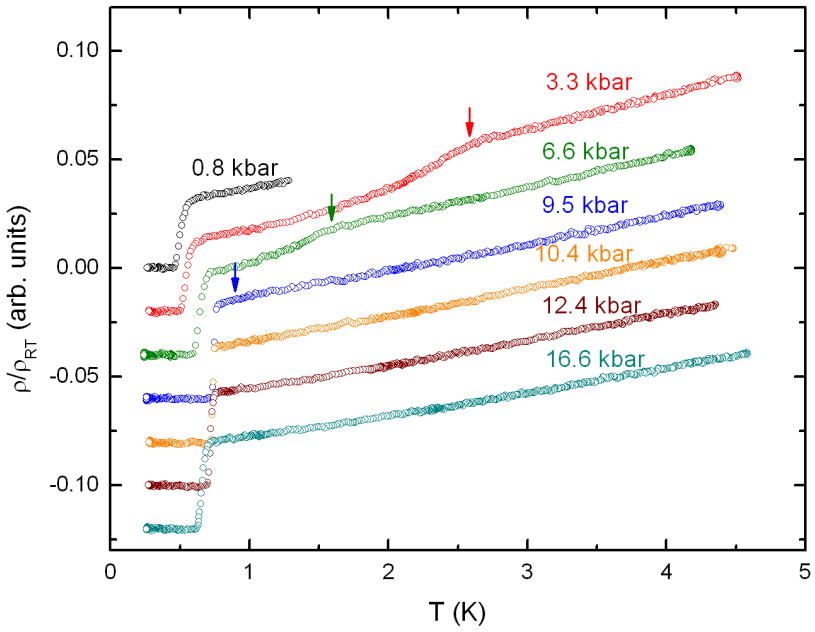

Figure 4.5: *The resistivity as a function of temperature at various pressures as indicated for $I \parallel a$.*

represent data measured for $I \parallel c$. The black symbols represent data that are taken in the ferromagnetic phase and the red symbols data taken in the paramagnetic phase. The blue circles are taken from Ref. [37]. The first four data points from Ref. [37] were taken in the magnetic region and should therefore be compared to the black triangles. The blue data points taken at pressures $p \gtrsim 8$ kbar are taken in the paramagnetic phase and should therefore be compared to the red data points. For the paramagnetic phase x is quite stable, with a slight upturn for $p > 15$ kbar. In the ferromagnetic phase x decreases rapidly with increasing pressure, much like the corresponding blue data points. We conclude that the qualitative behaviour of our samples is similar to that reported in Ref. [37].

The magnetic transition was measured in various magnetic fields at two pressures: 3.3 and 6.6 kbar. The data at 6.6 kbar were taken using an excitation current of 500 μA rather than the usual 100 μA, in order to reduce noise. No significant heating was observed. The magnetic field was increased in 0.25 T steps until further increasing B did not affect the resistivity curve. The magnetic field broadens the magnetic transition, it also slightly increases T_C. The data taken at 6.6 kbar are shown in figure 4.9. In order to determine T_C the difference with the highest field measurement (1.75 T) was taken and the resulting curve was smoothed using an adjacent averaging routine. The results are shown in figures 4.10 (3.3 kbar) and 4.11 (6.6 kbar). Taking the center of the peaks as T_C the T_C versus B curves shown in figure 4.12 are obtained. Both curves show the same qualitative behaviour. T_C increases as a function of magnetic field and then saturates at ~ 1.25 T. The change is weaker at higher pressure. This is possibly related to the decrease of the magnetic moment with pressure. In chapter 4.5 we will show that the upper critical field

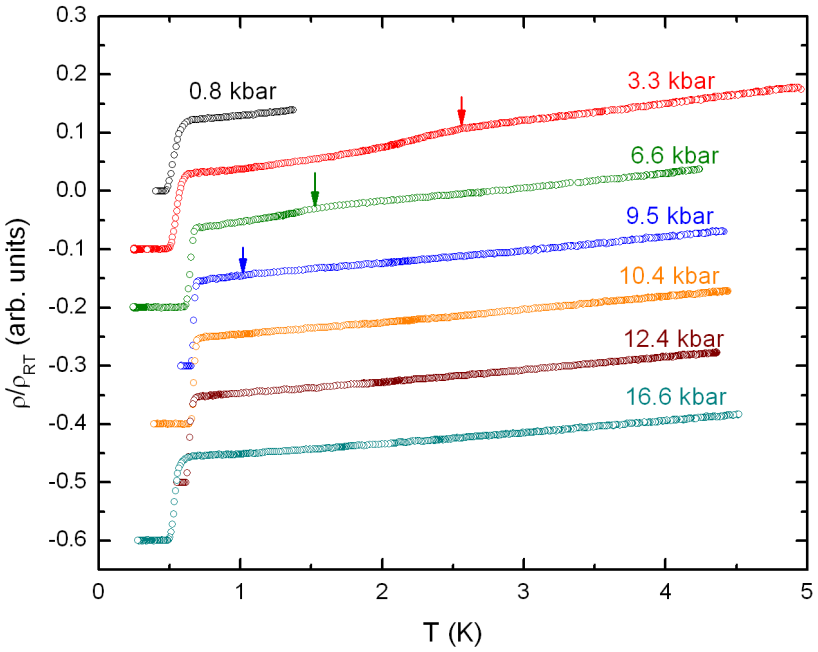

Figure 4.6: *The resistivity as a function of temperature at various pressures as indicated for $I \parallel c$.*

versus temperature curves show a change of curvature at a magnetic field of the same order of magnitude.

4.4 Phase Diagram

Using the magnetic and superconducting transition temperatures obtained from the AC-susceptibility and resistivity measurements we can construct the pressure-temperature phase diagram for UCoGe which is shown in figure 4.13. Resistivity is not a bulk probe whereas AC-susceptibility is a bulk property of the material. We will therefore use the AC-susceptibility data to indicate the different regions in the phase diagram. The blue and yellow circles indicate the magnetic and superconducting transitions, both measured by AC-susceptibility, respectively. The triangles pointing up and down are taken from a-axis and c-axis resistivity measurements respectively. The ambient pressure data (taken from Ref. [12]) are obtained from a polycrystalline sample by AC-susceptibility (symbol square).

The first point that should be noted is that superconductivity persists throughout the entire pressure range. It does not vanish together with the magnetism at the same critical point as would be expected from the generic phase diagram for ferromagnetic superconductors [21]. Superconductivity survives in the paramagnetic phase above the critical pressure and is enhanced near the critical point.

We note that the superconducting transition temperatures measured by resistivity are always higher than the ones measured by AC-susceptibility. This is in accordance with the previous observation [12] that the

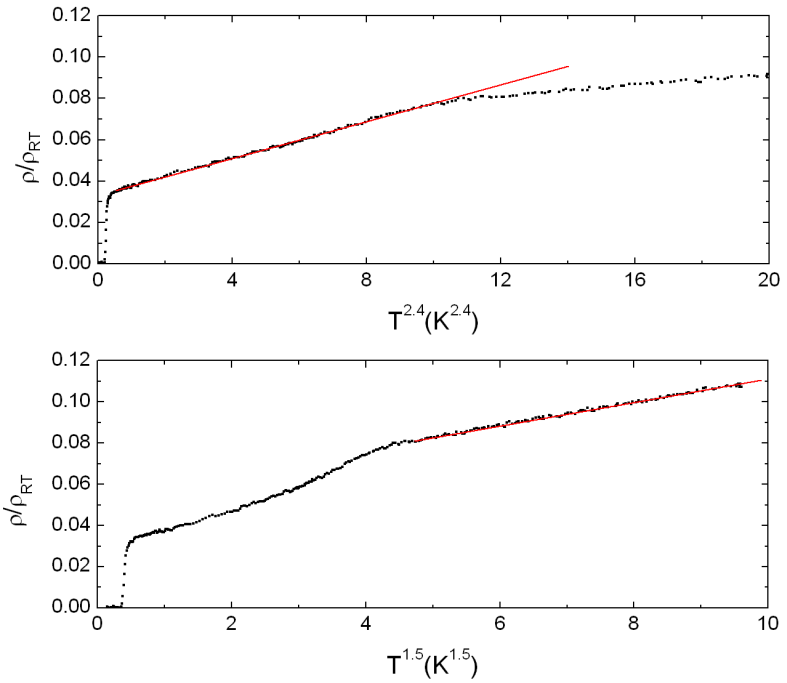

Figure 4.7: *An example of the procedure used to determine x in $\rho = \rho_0 + A_x T^x$. The normalised resistivity is plotted versus T^x at 3.3 kbar for $I \parallel a$. In the upper panel the ferromagnetic phase shows linear behaviour for $x = 2.4$ and in the lower panel the paramagnetic phase shows linear behaviour for $x = 1.5$, as indicated by the red lines.*

diamagnetic signal only appears when the resistive transition is complete. For $p < 8$ kbar T_{sc} increases quasi linearly with a slope of 0.03 K/kbar, which is slightly larger than the value predicted from the Ehrenfest relations (0.02 K/kbar).

For $p \gtrsim 4$ kbar the magnetic phase boundary decreases quasi-linearly and intersects the superconducting phase boundary near $p \approx 11.6$ kbar. The slope is equal to -0.24 ± 0.05 K/kbar, which is almost equal to the slope derived from the Ehrenfest relation (-0.25 K/kbar).

The magnetic transition is continuous over the entire pressure range, therefore we expect that ferromagnetic order vanishes at a second order quantum critical point at a pressure of $p_c \approx 14.0 \pm 0.5$ kbar. This value is obtained by linearly extrapolating T_C down to 0 K. An almost equal value ($p_c \approx 14.6 \pm 1.0$ kbar) is obtained by extrapolating the peak amplitude (shown in figure 4.14) down to zero. We cannot rule out however that the magnetism vanishes abruptly near $p \approx 11.1$ kbar. This would mean that the nature of transition changes and that the phase line terminates in a first order quantum end point [41].

The phase diagram obtained here is similar to the one shown in figure 4.2, which was obtained from a polycrystalline sample with relatively broad magnetic and superconducting transitions. Both phase dia-

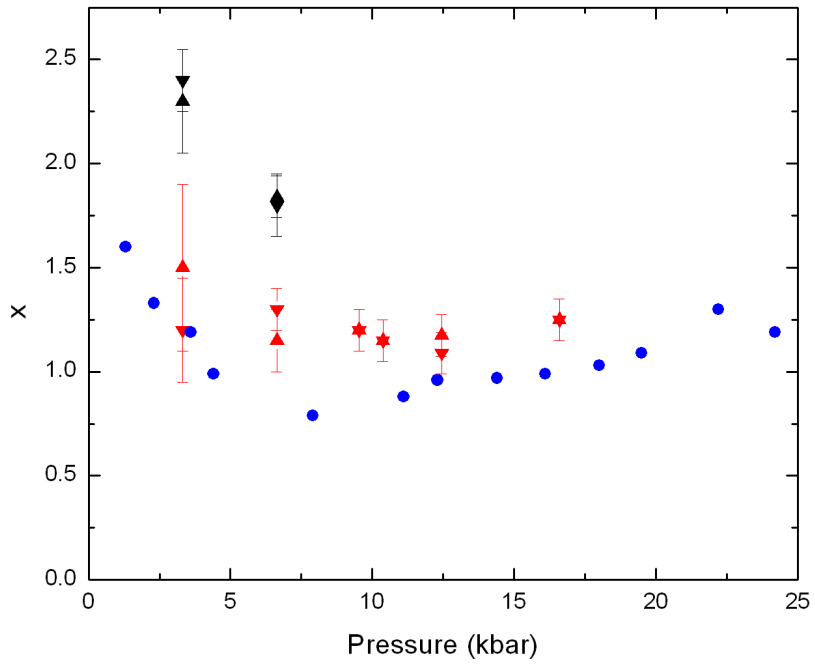

Figure 4.8: *The fit parameter x of a $\rho = \rho_0 + A_x T^x$ fit of the resistivity measurements. Triangles pointing up represent $I \parallel a$ and triangles pointing down represent $I \parallel c$. The black symbols are taken in the magnetic state and the red symbols are taken in the normal state. The blue circles are taken from Ref. [37] and were obtained for a polycrystalline sample.*

grams show that superconductivity persists up to the highest pressure and that T_C gradually decreases. There is a clear difference between the widths of the superconducting transition as a function of pressure however. This difference is striking especially in the pressure range above 12 kbar. In figure 4.15 the transition widths (black triangles) are plotted as a function of pressure together with the data of Ref. [37] (blue circles). The width of the bulk transitions (red triangles), measured by AC-susceptibility, have also been included. Such a strong increase of the superconducting transition width is likely caused by the fact that measurements were performed on a polycrystalline rather than a singlecrystalline sample. The grains in a polycrystalline sample give rise to a distribution of transition temperatures which results in broad transitions. The authors report that the onset temperature of superconductivity depends only very weakly on pressure (as shown in the inset of figure 4.2). In our work the onset temperature depends on pressure in the same way as the midpoint as can be seen in figures 4.5 and 4.6. Also the rapid increase in the width of the transition starting at 12 kbar is not observed in this work, although the high pressure region was not studied extensively by resistivity. There is no indication in our data however that would suggest such a sudden upturn and the superconducting transitions measured by AC-susceptibility show no such behaviour. Another notable difference is the slope at which magnetism is suppressed, which is

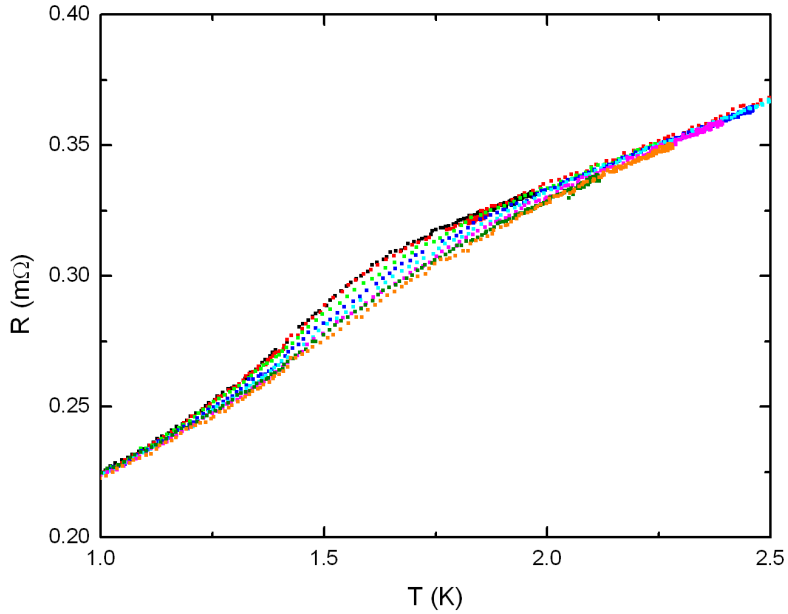

Figure 4.9: *The resistivity as a function of T around the magnetic transition for B ∥ I ∥ a measured in various magnetic fields. The fields range from 0 T (black curve) to 1.75 T (orange curve) and increase in steps of 0.25 T. These data have been taken at a pressure of 6.6 kbar.*

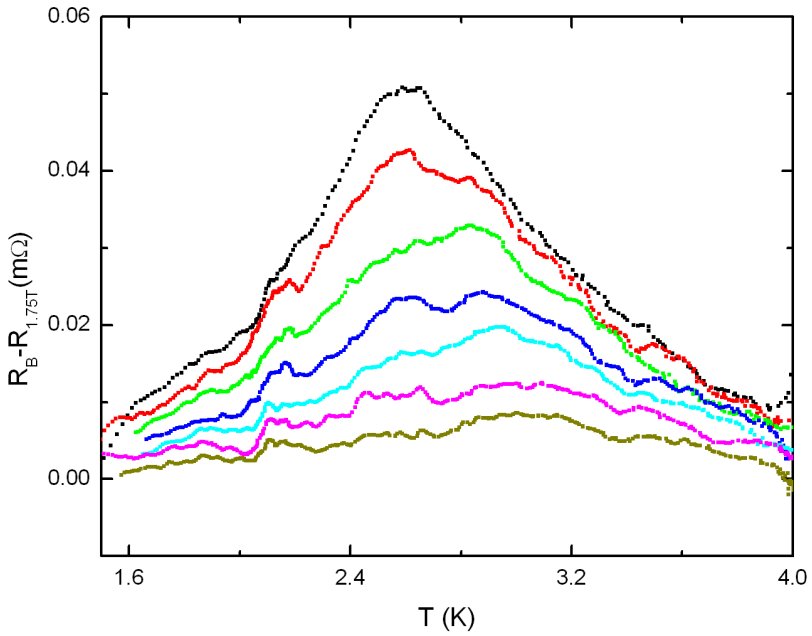

Figure 4.10: *The magnetic transition measured on the a-axis sample measured in various magnetic fields. The data at 1.75 T have been subtracted from the data at lower fields and the resulting curves have been smoothed using an adjacent averaging routine. The fields range from 0 T (black curve) to 1.5 T (olive curve) and increase in steps of 0.25 T. These data have been taken at a pressure of 3.3 kbar.*

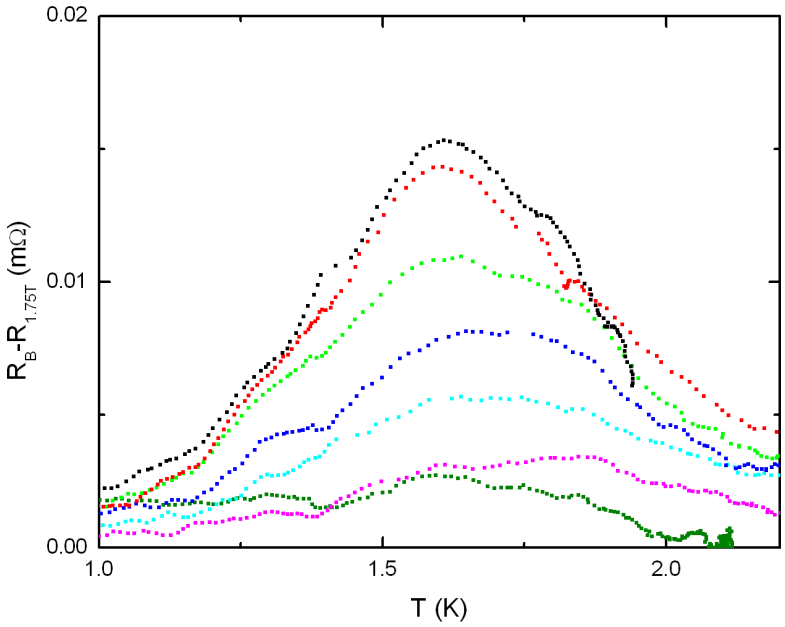

Figure 4.11: *The magnetic transition measured on the a-axis sample measured in various magnetic fields. The data at 1.75 T have been subtracted from the data at lower fields and the resulting curves have been smoothed using an adjacent averaging routine. The fields range from 0 T (black curve) to 1.5 T (olive curve) and increase in steps of 0.25 T. These data have been taken at a pressure of 6.6 kbar.*

-0.14 K/kbar compared to -0.24 K/kbar in this work. This is probably caused by the broadness of the magnetic transition, which makes precise determination of T_C difficult. The authors identify a characteristic pressure p^*, at which the superconducting transition temperature is highest. This is also the highest pressure at which magnetism can still be observed. We identify this pressure as $p = 11.6$ kbar, the pressure at which T_C drops below T_{sc}.

The phase diagram of UCoGe is qualitatively different than that of any other ferromagnetic superconductor. In UGe_2 ($T_C = 53$ K [9]) superconductivity is pressure induced and found only in the ferromagnetic region, much like in the generic phase diagram. Superconductivity is observed below 1 K in a limited pressure range on the border of ferromagnetism. At p_c (16-17 kbar) both magnetism and superconductivity disappear together. The transition at T_C becomes first order on approaching the critical pressure [42].

In UIr ($T_C = 46$ K [15]) there are three ferromagnetic regions in the pressure-temperature phase diagram. Superconductivity exists only in the third one (21-28 kbar near 0 K) in a pressure range of 26 to 28 kbar. Also here superconductivity and magnetism vanish together at the same critical pressure. The phase transition at T_C remains second order all the way to $T \rightarrow 0$ [15].

The only other ambient pressure ferromagnetic superconductor is URhGe ($T_C = 9.5$ K, $T_{sc} = 0.25$ at

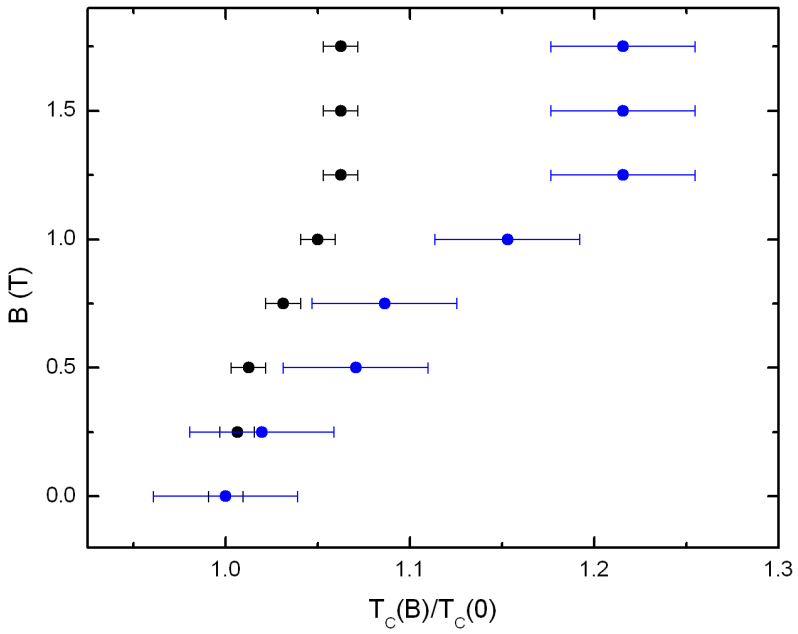

Figure 4.12: *T_C as a function of magnetic field at a pressure of 3.3 kbar (blue symbols) and 6.6 kbar (black symbols). T_C has been normalised to 1 at zero field.*

ambient pressure [11]). But applying pressure to this material raises T_C and drives the system away from the magnetic instability [16].

None of these materials have a superconducting phase in the paramagnetic region, this makes UCoGe unique. In chapter 2.2 the possible symmetry classes for the different regions of the phase diagram were discussed. Since the superconducting state in the paramagnetic region (S_2) does not break time reversal symmetry it could be either a conventional singlet state or a triplet state. One could argue that because T_{sc} does not change drastically when crossing p_c it is highly unlikely that the nature of the state changes from a triplet to a singlet state. However from a phase diagram alone we cannot make such a statement with certainty. But if S_2 is a singlet state its critical field should obey the Pauli paramagnetic limit for singlet superconductivity $B_{c2}^{Pauli} \approx 1.83 \times T_{sc} \approx 1.3$ T [25]. The upper critical field $B_{c2}(0)$ at ambient pressure was found to be approximately 5 T [26], providing evidence for triplet superconductivity at ambient pressure. Consequently if UCoGe is a singlet superconductor when the pressure is raised above p_c a large drop in the upper critical field should be observed. By measuring the upper critical field we will be able to determine whether S_2 is a singlet or a triplet superconducting state.

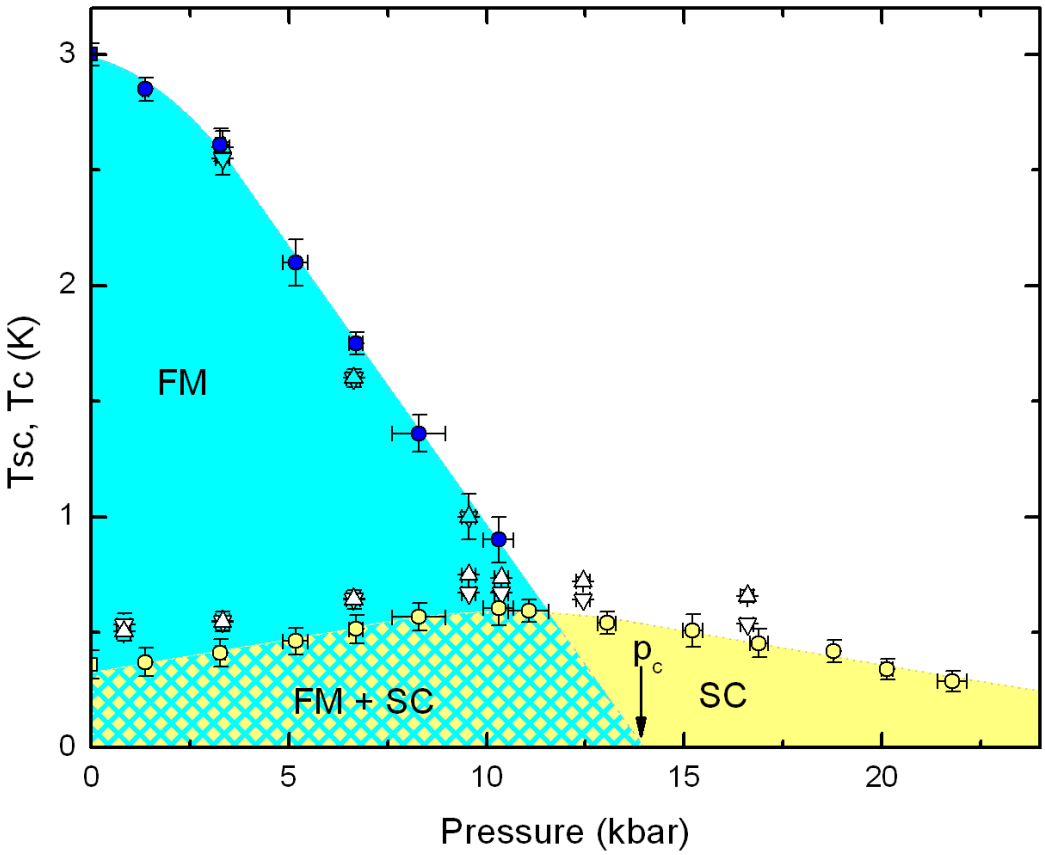

Figure 4.13: *The UCoGe pressure-temperature phase diagram constructed from AC-susceptibility and resistivity measurements. T_C versus pressure measured by AC-susceptibility is represented by blue circles. The cyan triangles pointing up and down represent T_C versus pressure measured by resistivity for $I \parallel a$ and $I \parallel c$ respectively. T_{sc} versus pressure measured by AC-susceptibility is represented by yellow circles. The white triangles pointing up and down represent T_{sc} versus pressure measured by resistivity for $I \parallel a$ and $I \parallel c$ respectively. FM: ferromagnetic phase. FM + SC: ferromagnetic superconducting phase (S_1). SC: superconducting phase (S_2).*

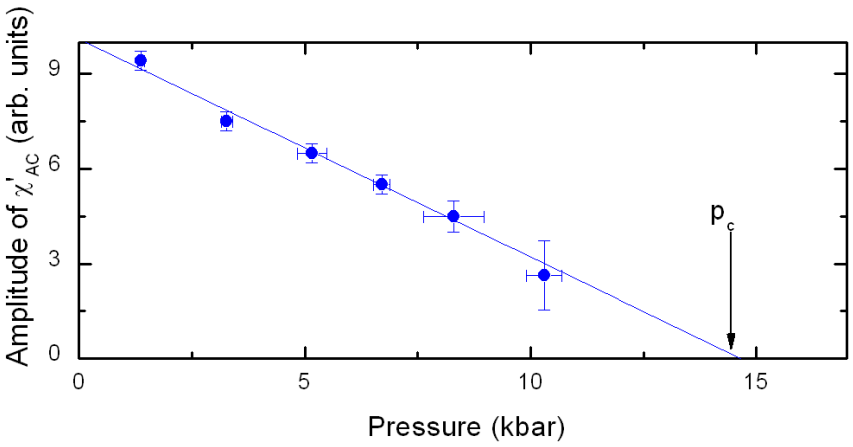

Figure 4.14: *The amplitude of the peak measured at the magnetic transition in AC-susceptibility as a function of pressure. Extrapolating the amplitude down to zero yields a critical pressure of* 14.6 ± 1.0 *kbar.*

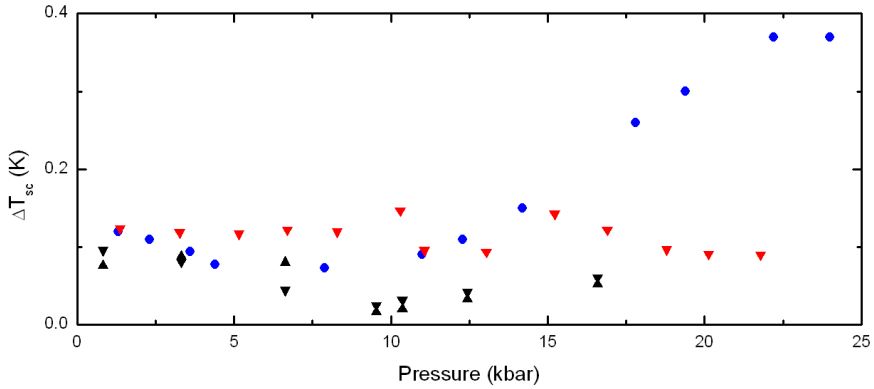

Figure 4.15: *The superconducting transition width as a function of pressure. The black triangles pointing up are data taken for the a-axis sample and the triangles pointing down are data taken for the c-axis sample. The red triangles are taken from the AC-susceptibility data. The blue circles are data points taken for a polycrystal from Ref. [37]*

4.5 Critical field

The critical field as a function of pressure was studied by resistivity measurements. The superconducting transition was measured for $B \parallel I \parallel a$ and $B \parallel I \parallel c$ in various fields. An example of such a measurement is shown in figure 4.16 for $B \parallel I \parallel a$ and in figure 4.17 for $B \parallel I \parallel c$. Both examples are for $p = 10.4$ kbar. Note that the widths of the transitions decrease with increasing field. For $B \parallel I \parallel c$ a double superconducting transition is observed for $B > 0.2$ T. This has been observed at every pressure $p \geqq 9.5$ kbar. Considering the low RRR of this sample (~ 7 at ambient pressure) we cannot exclude that this field induced double transition is due to inhomogeneities in the sample. By taking the midpoint of the transition as T_{sc} for each magnetic field and each pressure we can construct the magnetic field-temperature phase diagram for each pressure. The data are shown in figure 4.18. Included are ambient pressure measurements taken from Ref. [26] (also shown in figure 4.1), which were taken on the same sample as our $B \parallel a$ measurements. The open symbols represent data taken for $B \parallel I \parallel c$ and the closed symbols represent data taken for $B \parallel I \parallel a$. The inset shows the magnetic field at which the superconducting transition temperature of the a-axis sample is 0.6 or 0.8 times its value at zero field.

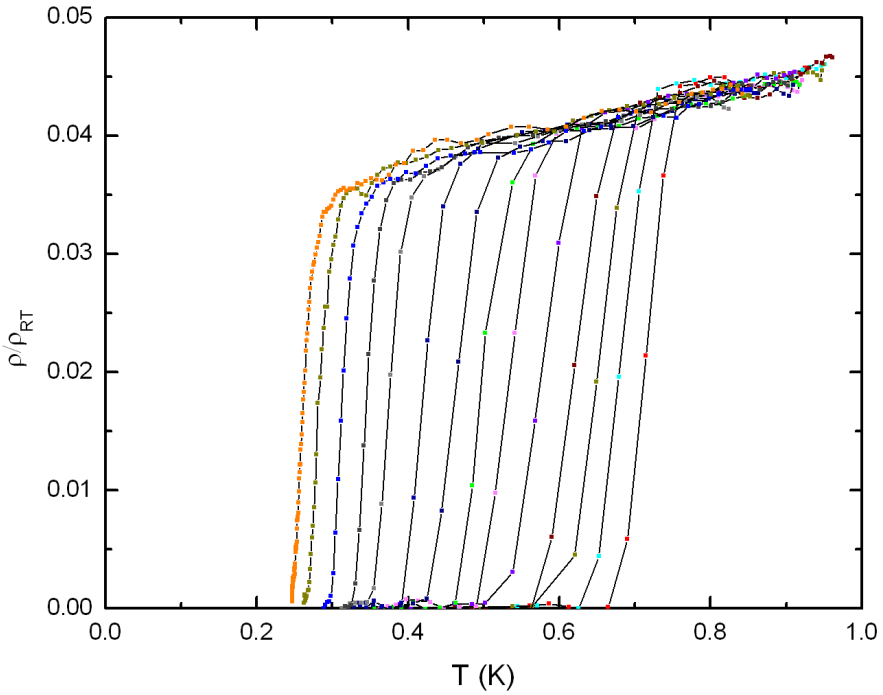

Figure 4.16: *Temperature variation of the resistivity of single crystalline UCoGe for $B \parallel a$ in various magnetic fields at $p = 10.4$ kbar. At this pressure 56 curves were measured, here we show 14. The fields at which these transitions were measured are from right to left: 0.05, 0.3, 0.6, 0.9, 1.4, 2.0, 2.4, 3.0, 3.8, 4.8, 5.6, 6.4, 7.2 and 7.8 T.*

Applying pressure strongly enhances the critical field of UCoGe even though T_{sc} changes only very little.

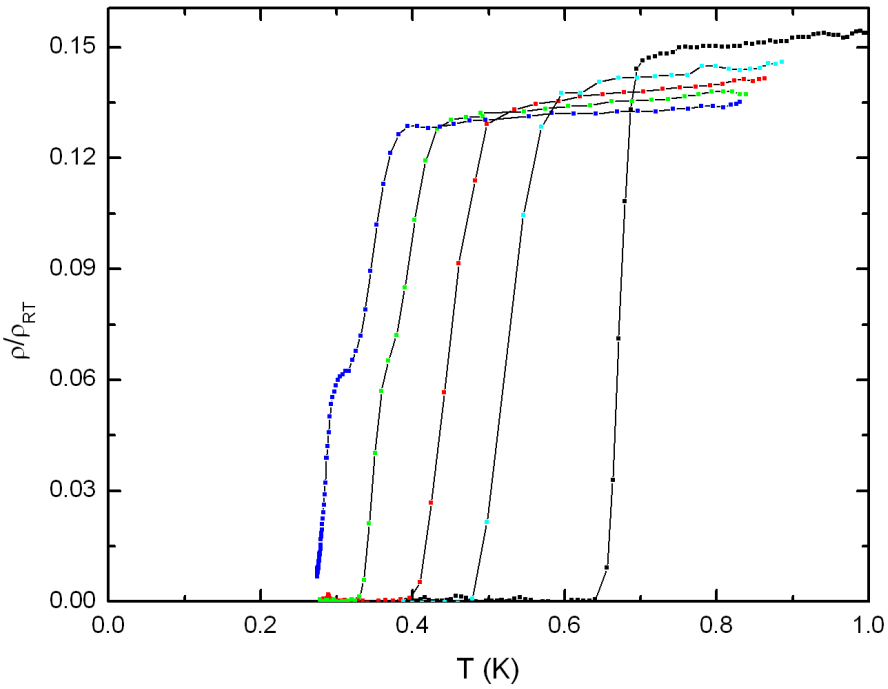

Figure 4.17: *Temperature variation of the resistivity of single crystalline UCoGe for $B \parallel c$ in various magnetic fields at $p = 10.4$ kbar. The fields at which these transitions were measured are from right to left: 0.0, 0.05, 0.1, 0.2 and 0.3 T.*

Near p_c $B_{c2}(0)$ can be as high as 15 T, which exceeds the ambient pressure value by a factor 3, while T_{sc} increases by only 40%. $B_{c2}(0)$ remains large throughout the entire pressure range measured. This proves that the superconducting state in the paramagnetic region cannot be a conventional singlet state, because the Pauli paramagnetic limit is much lower than the critical field that is measured. Therefore we conclude that this state is also a triplet state. A planar state analogous to that of liquid ^{3}He is the best candidate.

The B_{c2} curves show no sign of saturation and the upward curvature, which was already observed in Ref. [26], is even more pronounced under pressure. A fit of the curves has been made using a phenomenological formula which was also used in Ref. [43] in a similar situation where the upper critical field curves of $Y_xLu_{1-x}Ni_2B_2C$ showed upward curvature.

$$B_{c2}(T) = B_{c2}(0)\left(1 - \frac{T}{T_{sc}}\right)^{1+\alpha} \tag{4.1}$$

An example of such a fit is shown in figure 4.19 for the 10.4 kbar measurement. The black line represents a fit taken with in a range of 0 T to the highest field (7.8 T). Above 2 T the result is in good agreement with the data, but at lower fields the fit deviates strongly from the data. Because of this we fitted between

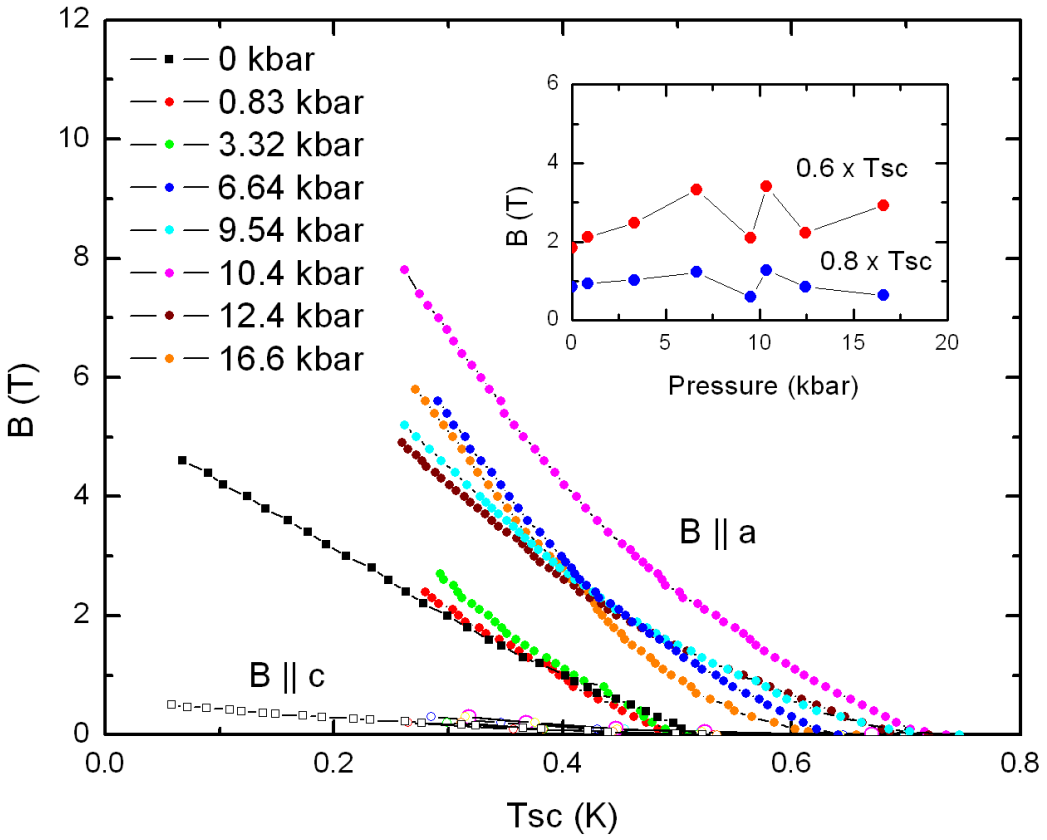

Figure 4.18: *The field-temperature phase diagram for UCoGe measured by resistivity for all pressures. The ambient pressure data (squares) are taken from [26] on the same sample. The open symbols are for $B \parallel c$ and $I \parallel c$ and the closed symbols are for $B \parallel a$ and $I \parallel a$. The inset shows the magnetic field at which the superconducting transition temperature is 0.6 or 0.8 times its value at zero field.*

0 and 2 T separately. This fit is represented by the cyan line in figure 4.18. It has been extrapolated to higher fields. In figure 4.20 the parameter α of the B_{c2} curves have been plotted for low fields (< 2 T, black symbols) and high fields (> 2 T, red symbols). The parameter α is a measure of the curvature of the plot and it can be seen that α increases from 0.1 at a low pressure to ~ 1 at 6.6 kbar for low fields after which it seems to be constant. This clearly shows that the largest contribution to the increasing upward curvature comes from the low field region. The change of curvature takes place at a field ~ 2 T for each data set. The high field region also shows some increase in curvature, but it is not nearly as strong as the low field region. In section 4.3 we showed the effect of a magnetic field on the magnetic transition. T_C increases as a function of field until a field of ~ 1.25 T is reached, above which T_C saturates. The fact that these two fields are very similar in magnitude hints at a correlation between these two effects. More accurate measurements of T_C as a function of B, for instance by measuring AC-susceptibility rather than resistivity, may shed more light on this. Extrapolating the high field fits down to T = 0 gives an estimate

for $B_{c2,a}(0)$ as a function of pressure. These conservative estimates are shown in table 4.1.

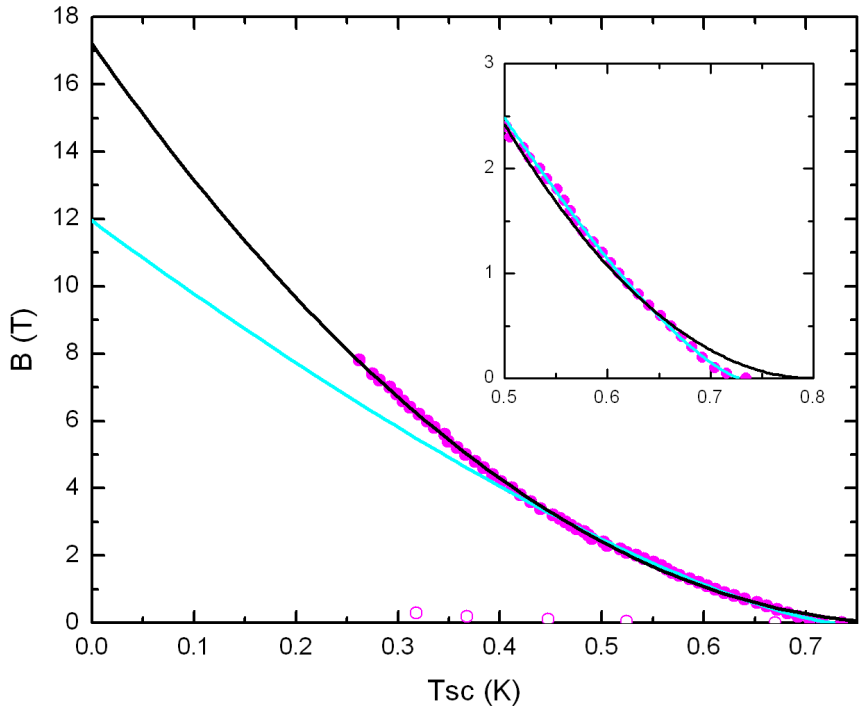

Figure 4.19: *Example of a fit using equation 4.1 for* $p = 10.4kbar$*. The black line represents a fit done over the entire magnetic field range. This fit is in good agreement with the data for* $B > 2$ *T. For lower fields however the data deviates strongly as can be seen in the insert in which we zoom in on the low field range. The cyan line represents a fit between 0 and 2 T which has been extrapolated to higher fields.*

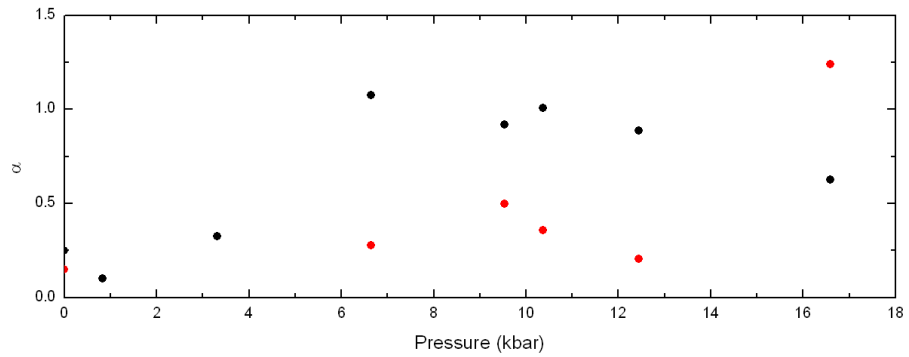

Figure 4.20: *The parameter* α *from a* $B_{c2} = B_{c2}(0)\left(1 - \frac{T}{T_C}\right)^{1+\alpha}$ *fit to the* B_{c2} *curves. The black symbols are taken for fields below 2 T and the red symbols are taken for fields above 2 T.*

Such upward curvature would normally be a sign of two (or multiple)-band superconductivity in 3D materials [44]. In this instance it could be attributed to a field induced population redistribution of spin up and spin down bands. However, when the pressure is raised above the critical pressure, magnetism

Pressure (kbar)	$B_{c2}(0)$ (T)
0	5
0.83	6
3.32	8
6.63	17
9.54	12
10.4	17
12.4	11
16.6	15

Table 4.1: *The estimated values of* $B_{c2}(0)$ *for each pressure.*

disappears and these bands become degenerate, leaving only one superconducting band. Mineev and Champel [38] have evaluated the linearized Ginzburg-Landau equations including gradient terms for a cubic two-band ferromagnetic superconductor with gaps $\Delta_{\uparrow\uparrow}$ and $\Delta_{\downarrow\downarrow}$. Depending on the strength of the pairing interactions and some anisotropy constants an upturn in B_{c2} is predicted. Because of this an upturn in the orthorhombic case would also seem likely, but calculations for this situation have not been done however. Such calculations may shed more light on this unusual behaviour.

5 Conclusion

AC-susceptibility and resistivity measurements have been performed on single crystalline UCoGe samples under pressure. T_C and T_{sc} have been extracted from every measurement and the pressure temperature phase diagram has been constructed. Magnetism is suppressed with a slope of -0.24 K/kbar and vanishes at a critical pressure of $p_c = 14$ kbar. T_{sc} increases at first with a slope of 0.03 K/kbar until it reaches a maximum of 604 mK in AC-susceptibility at $p^* = 11.6$ kbar, the pressure at which the superconducting phase line intersects the magnetic phase line. After this T_{sc} decreases steadily, but never vanishes. In the resistivity measurements T_{sc} has a maximum of 750 mK for $I \parallel a$ and 670 mK for $I \parallel c$ at p^*. Superconductivity persists throughout the entire pressure range measured (up to 22 kbar). This makes UCoGe unique: no other ferromagnetic superconductor has a superconducting state in the paramagnetic region of the phase diagram. Upper critical field measurements show a strong enhancement of superconductivity near the critical pressure. $B_{c2}(0)$ attains three times its ambient pressure value and T_{sc} is increased by 40%. Also above the critical pressure B_{c2} remains large providing evidence for a triplet superconducting state in the paramagnetic region similar to the planar phase of liquid ^{3}He.

A study of T_C as a function of external field showed an increase of T_C up to a field of ~ 1.25 T above which T_C saturated. The change in T_C becomes weaker with pressure which could possibly be explained by the decrease in the magnetic moment with pressure.

The curvature in $B_{c2}(T)$ which was already measured at ambient pressure shows strong enhancement with pressure. A change of curvature was measured for fields above ~ 2 T. As this is in the same order of magnitude as the field for which T_C no longer increases these two effects might be related.

The anisotropy in the upper critical field ($B^a_{c2} \gg B^c_{c2}$) which was already measured at ambient pressure is also preserved. This provides evidence for a superconducting gap structure with axial symmetry for the entire pressure range measured.

An obvious next step in this research would be to measure the upper critical field down to lower temperatures in a dilution fridge. Doing so would allow one to determine whether the upward curvature persists at lower temperatures or the critical field curves will level off. It will also allow one to make more accurate estimates of $B_{c2}(0)$. Also more accurate measurements of the effect of a magnetic field on the magnetic transition as a function of pressure might shed more light on the change of curvature at around 2 T in the upper critical field curves. This can for instance be done by measuring AC-susceptibility with $B \parallel a$.

We conclude that the p-T-B phase diagram of UCoGe provides a unique opportunity to investigate unconventional superconductivity stimulated by magnetic interactions.

6 Acknowledgments

Massive appreciation to the following exalted members of the human race: Anne, thank you for giving me the opportunity to be a part of this group and its research. You are a great and patient teacher and I learned a great deal from you. Takashi, thank you for supplying the high pressure equipment and teaching me how to use it. Without you this would have been a completely different thesis. Also, thanks for the Japanese cookies, even though they taste quite funny with coffee. Alessia, my sweet 'sister', thank you for teaching me how to use all the other experimental equipment without destroying anything expensive. Working with you was a blast and thank you for keeping me well fed. Meena, even though we are in the same group we never did much work together, nevertheless you definitely increased the fun-factor for me during the past year.

There are many people in the WZI to whom I owe thanks and if I make the attempt to mention them all I will probably forget some. Therefore I will just thank everyone for their help, their feedback and the great atmosphere. I also want to use this opportunity to apologise to anyone who was ever bothered by the music I like to listen to while working. What can I say? There is nothing like the combination of drums and guitars pounding and chugging away to get the brain going. I hope it was not too much of a bother to anyone, if it was: my apologies.

I want to thank my parents, my brother and his girlfriend for their great support and for making the past year a whole lot easier for me. I want to thank my friends for countless hours of conversation about basically nothing. May our quarter pounders be ever warm and tasty. To all friends with whom I do not eat quarter pounders (very often): I thank you as well. And last but not least: my band Alantia for helping me get what I need for my decibel addiction in a safe and secure environment. Soon we will conquer the world, whether the world is ready for that or not. All readers are encouraged to have a look (and especially a listen!) at Ref. [45].

"We were different, just like all the other kids...."

Bad Religion - You Don't Belong (2002)

References

[1] H. Kamerlingh Onnes *et al. Comm. Phys. Lab. Univ. Leiden* Nos. 122 and 124, (1911).

[2] L.N. Cooper J. Bardeen and J.R. Schrieffer. *Phys. Rev.* **106** 162-164 (1957).

[3] J. G. Bednorz and K.A. Müller. *Z. Phys. B* **64** (1957) 189-193.

[4] B.T. Matthias *et al. Phys. Rev. Lett.* **1** (1958) 92-94.

[5] Ø. Fischer. *Appl. Phys.* **16** (1978) 1.

[6] R.J. Cava *et al. Nature (London)* **367** (1994) 252.

[7] M.B. Maple *et al. Crystalline electric field and structural effects in f-electron systems* (Plenum, New York, 1980) p.533.

[8] F. Steglich *et al. Physica B+C* **126** (1984) 82.

[9] S.S. Saxena *et al. Nature* **406** (2000) 587-592.

[10] T. Akazawa *et al. J. Phys.: Condens Matter* **16** (2004) L29.

[11] F. Hardy and A. D. Huxley. *Phys. Rev. Lett.* **94** (2005) 247006.

[12] N. Huy *et al. Phys. Rev. Lett.* **99** (2007) 067006.

[13] N.D. Mathur *et al. Nature* **394** (1998) 39.

[14] C. Pfleiderer and A.D. Huxley. *Phys. Rev. Lett.* **89** (2002) 147005.

[15] T. C. Kobayashi *et al. Physica B.* 378-380 (2006) 355-358.

[16] F. Hardy *et al. Physica B* **359-361** (2005) 1111-1113.

[17] G.G. Lonzarich and L. Taillefer. *J. Phys. C: Solid State Phys.* **18** (1985) 4339.

[18] A. de Visser *et al. Phys. Rev. Lett.* **102** (2009) 167003.

[19] N. T. Huy. *Ph.D thesis*(University of Amsterdam, 2008) *unpublished.*

[20] G. G. Lonzarich. *Electron, a centenary volume*, (Cambridge University Press, Cambridge, 1997), Chapter 6.

[21] D. Fay and J. Appel. *Phys. Rev. B* **22** (1980) 3173.

[22] T.R. Kirkpatrick *et al. Phys. Rev. Lett.* **87** (2001) 127003.

[23] V.P. Mineev. *ArXiv:* 0812.2171v1 (2008).

[24] V.P. Mineev and K. V. Samokhin. *Introduction to Superconductivity* (Gordon and Breach Science Publisheres, Amsterdam, 1999).

[25] A.M. Clogston. *Phys. Rev. Lett.* **9** (1962) 266.

[26] N. Huy *et al. Phys. Rev. Lett.* **100** (2008) 077002.

[27] I.A. Fomin. *JETP Lett* **74** (2001) 111.

[28] V.P. Mineev. *Phys. Rev. B.* **66** (2002) 134504.

[29] K. Scharnberg and R.A. Klemm. *Phys. Rev. Lett.* **54** (1985) 2445.

[30] K. Scharnberg and R.A. Klemm. *Phys. Rev. B.* **22** (1980) 5233.

[31] T. Naka. *private communications.*

[32] K. Murata *et al. Rev. Sci. Instrum.* **68** (1997) 2490.

[33] B. Bireckoven and J. Wittig. *J. Phys. E: Sci. Instrum.* **21** (1988) 841.

[34] F. Pobell. *Matter and methods at low temperatures* (Springer-Verlag, 1992), Chapter 6.

[35] www.oxford-instruments.com.

[36] A.F. Deutz *et al. Rev. Sci. Instrum.* **60** (1988) 113.

[37] E. Hassinger *et al. J. Phys. Soc. Jpn* **77** (2008) 073703.

[38] V.P. Mineev and T. Champel. *Phys. Rev. B.* **69** (2004) 144521.

[39] N. Doiron-Leyraud *et al. Nature* **425** (2003) 595.

[40] S. Takashima *et al. J. Phys. Soc. Jpn.* **76** (2007) 043704.

[41] D. Belitz *et al. Phys. Rev. Lett.* **82** (1999) 4707-4710.

[42] T. Terashima *et al. Phys. Rev. Lett.* **87** (2001) 166401-1:4.

[43] J. Freudenberger *et al. Physica C* **306** (1998) 1-6.

[44] S.V. Shulga *et al. Phys. Rev. Lett.* **80** (1998) 1730-1733.

[45] www.myspace.com/alantiamusic.